A simple yet effective ALE-FE method for the nonlinear planar dynamics of variable-length flexible rods

P. Koutsogiannakis[1], T.K. Papathanasiou[2] and F. Dal Corso[1*]

[1] *DICAM, University of Trento, via Mesiano 77, Trento, Italy*

[2] *Department of Civil Engineering, Aston University, Birmingham B4 7ET, UK*

Abstract

With recent advances in variable-length structures for use in soft actuation, energy harvesting, energy dissipation and metamaterials, the mathematical modelling and numerical simulation of physical systems with time-varying domains is becoming increasingly important. The planar nonlinear dynamics of one-dimensional elastic structures with variable domain is formulated from a Lagrangian approach by using a non-material reference frame. An Arbitrary Lagrangian-Eulerian (ALE) scheme is proposed where the domain is reparametrized based on a priori unknown configuration parameters. Based on this formulation, a Finite Element (FE) method is developed for theoretically predicting the evolution of a rod constrained at its ends by one or two sliding-sleeves, whose position and inclination can be varied in time, and under external loadings. Finally, case studies and instability problems are investigated to assess the reliability of the proposed formulation against others available and to demonstrate its effectiveness. With respect to previously developed methods for this type of structural problems, the present ALE-FE approach shows a strong theoretical and implementation simplicity, maintaining an efficient and fast convergence according to the cases analyzed. An open source code realized for the present ALE-FE model is made available for solving the nonlinear dynamics of planar systems constrained by one or two independent sliding sleeves. The present research paves the way for further extensions to easily implement solvers for the three-dimensional dynamics of flexible one- and two-dimensional structural systems with moving boundary conditions.

Keywords: Configurational forces; sliding-sleeve; nonlinear structural dynamics.

Nomenclature

ALE	Arbitrary Lagrangian-Eulerian		$\mathcal{N}$	Set of all non-constrained material points
FEM	Finite Element Method			
$\mathbf{p}$	Vector collecting all configuration parameters		$\mathcal{C}_i$	Set of all material points kinematically constrained by the i-th sliding sleeve
s_i	Configuration parameter denoting the exit of the i-th sliding sleeve		$\mathcal{L}$	Lagrangian of the structural system
s	Arc-length spatial variable		$\mathcal{F}$	Integrant function appearing in definition of $\mathcal{L}$
σ	Auxiliary spatial variable		$\mathcal{B}$	Space-independent terms of $\mathcal{L}$

*Corresponding author: francesco.dalcorso@unitn.it

$\mathcal{L}_{\mathcal{N}}$	Terms of the Lagrangian $\mathcal{L}$ associated with domain $\mathcal{N}$	$\mathbf{F}_q$	External forces acting on rod
$\mathcal{L}_{\mathcal{C}_i}$	Terms of the Lagrangian $\mathcal{L}$ associated with domain $\mathcal{C}_i$	$\mathbf{x}$	Position of the centerline of the rod
$\mathcal{E}$	Total energy of structural system	N	Lagrange multiplier associated with inextensibility constraint
$\mathcal{E}_{\mathcal{N}}$	Energy associated to non-constrained portion of rod	$\mathbf{R}_i$	Lagrange multiplier associated with continuity of rod at i-th sliding sleeve exit
$\mathcal{E}_{C_i}$	Energy associated to portion of rod inside i-th sliding sleeve	M_i	Lagrange multiplier associated with continuity of the spatial derivative of the rod centerline at i-th sliding sleeve exit
$\mathcal{T}$	Kinetic energy of the structural system	$\mathbf{C}_i$	Concentrated force at i-th sliding sleeve exit
$\mathcal{T}_{\mathcal{N}}$	Kinetic energy of unconstrained portion of rod	$\mathbf{H}$	Interpolation matrix of field $\mathbf{x}$
$\mathcal{T}_{\mathcal{C}_i}$	Kinetic energy of rod portion inside i-th sliding sleeve	$\mathbf{P}$	Interpolation matrix of field N
		$\mathcal{A}$	The assembly operator of the Finite Element Method
$\mathcal{V}$	Potential energy of the structural system	$\hat{\mathbf{x}}$	Collection of degrees of freedom associated with field $\mathbf{x}$
$\mathcal{V}_{\mathcal{N}}$	Potential energy of unconstrained portion of rod	$\hat{\mathbf{c}}$	Collection of degrees of freedom associated with constraints and Lagrange Multipliers
$\mathcal{V}_{\mathcal{C}_i}$	Potential energy of rod portion inside i-th sliding sleeve	$(\cdot)^T$	Transpose of vector or matrix
$\mathcal{W}$	Work of external forces	β_1, β_2	Newmark method parameters
$\boldsymbol{\xi}$	Collection of fields and their space derivatives	$\mathbf{J}$	Jacobian matrix of discretized system of equations
$\delta(\cdot)$	First variation of a quantity	N_{el}	Number of elements in discretization
$(\dot{\cdot})$	First time derivative	B	Bending stiffness of rod
$(\ddot{\cdot})$	Second time derivative	γ	Linear mass density of rod
$(\cdot)_{,z}$	Derivative of quantity w.r.t z	L	Total length of the rod
$\frac{\mathrm{D}(\cdot)}{\mathrm{D}t}$	Material time derivative	m	Mass at free end of rod
j	Jacobian of auxiliary transformation $s(\sigma)$	$\mathbf{g}$	Gravity vector
		ℓ_0	Initial length of rod outside sliding sleeve
δ_{ij}	Kronecker delta	ω	Angular velocity of sleeve rotation
$\mathbf{a}_i$	Exit position of i-th sliding sleeve	c	Dissipation coefficient
$\mathbf{b}_i$	Unit vector parallel to i-th sliding sleeve	ζ	Non-dimensional dissipation coefficient
$\mathbf{n}_i$	Unit vector normal to i-th sliding sleeve	μ	Friction coefficient
θ_i	Angle between i-th sliding sleeve and x_1-axis		

1 Introduction

At multiple scales, deployable and reconfigurable structures are the key to realising adaptive devices capable of solving engineering problems ranging from geometric constraints in transport or in working conditions and of exhibiting improved mechanical properties in response to varying loading stimuli through dramatic shape morphing. These types of structures can be designed by using origami concepts [1, 2, 3], programmable metamaterials [4, 5, 6], or highly flexible elements [7, 8, 9]. With regard to the latter approach, the modelling of flexible structures of varying length is attracting increasing interest due to their recent connection with configurational mechanics, a theoretical framework introduced by Eshelby [10, 11] for analysing possible changes in the configuration of a solid, as for example due to a crack propagation.

Describing the deformed configuration of a variable length system requires adding one or more configuration parameters to the kinematics of the deformed part. In the case of a flexible rod partially constrained by a rigid and frictionless sliding sleeve, the configuration parameter is the relative position of the sliding sleeve exit along the rod. The sliding sleeve exit represents a *moving boundary* where a discontinuity in the curvature occurs and an unexpected non-null sliding reaction force is realized, which is concentrated at the sliding-sleeve exit and has an outward direction [12]. For this particular class of structural systems, this reaction force has been independently derived by both variational and micromechanical approaches and found to be the Newtonian expression of the Eshelby force on the structural system. The occurrence of a curvature jump at each sliding sleeve exit makes the dynamics of the rod undergoing large rotations very fast and interesting in certain instances of the phenomenon studied.

Moving boundary problems are of practical interest for several technological applications, as for example in passive self-tuning [13, 14, 15], in oil and gas industries [16, 17], in micro electro-mechanical systems [18, 19], soft robotics [20, 21, 22], in vibration control [23], in coiling [24] and injection [25] processes, and in medical catheterization [26, 27]. In the last decade, research into the configurational mechanics of structures has led to the realisation of measuring devices [28] and of self-tunable systems [29], as well to the establishment of novel actuation [30, 31] and buckling [32] principles. In addition, these advances have led to new insights into the configurational mechanics of solids for the interpretation of dislocation motion and crack advance [33], blistering [34, 35], delamination [36], penetration [37], and ejection [38] phenomena.

When structures with variable length are simulated with fine grained models, involving the solution of the full continuum problem and the solid-solid interaction between the rod and the sliding-sleeve, the simulations become computationally expensive as very fine 3D meshes are needed to capture accurately the frictionless contact reaction. Indeed, the relative sliding between the rod and the sliding sleeve constraint implies that the contact domain is continuously evolving in time and, as a result, any computational model needs to take this into account and proper remeshing strategies have to be implemented at every time step. In classical Finite Element (FE) models the mesh is updated at the beginning of every timestep and assumed constant for the entire step. This creates a time-discrete solution having incompatibilities with the time-continuous evolution of the domain and therefore the stability and convergence of such models is not guaranteed.

A natural way for overcoming these issues is the adoption of a non-material description of kinematic quantities, in analogy with the methods used in fluid mechanics [39]. Generally, an Arbitrary Lagrangian-Eulerian (ALE), also known as Mixed Eulerian-Lagrangian, formulation can be adopted, where an underlying transformation is arbitrarily chosen, mapping the variable physical domain to a normalized auxiliary domain that remains constant in time (Fig. 1). As a result, the mesh, defined on the normalized domain, becomes continuously variable in time when transformed to the material domain. This means that for quantities defined on material points, any time derivatives have to take into account the transformation of the domain, and equivalently that *material derivatives* have to be used, similarly to the Eulerian formulation in fluid mechanics and fluid-structure interaction [40, 41, 42].

So far, applications have been mainly solved within the category of axially moving structures with prescribed boundary motion [43], such as that realized in belt and pulleys mechanisms [44, 45, 46] and in the roll forming of metal sheets [47]. A non-material framework for the solution of structural problems with variable-domains has been introduced in [48] for the simulation of the spaghetti and inverse spaghetti problems where a rod is partially inserted in one sliding sleeve and the length of the rod inside the sliding-sleeve is controlled in time, further developed in [49]. An extensive overview on non-material formulations for this problem category has been presented in [50].

With regard to moving boundary problems with unprescribed motion, recently Boyer et al. presented an ALE framework for the simulation of inextensible Kirchhoff rods constrained by one sliding-sleeve using an extended Hamilton's principle [51], based on ideas found in [52, 53].[1] An ALE method has been also used to study the characteristic example of the dancing rod [55], extending the analysis of a rod's fall within a gravitational field [56] by considering a distributed mass. Furthermore, it has also been used for the configurational dynamics involving a

---

[1]According to [54], it is expected that the Hamilton-Jacobi theory cannot be properly used for the problem under consideration since the incompleteness of this theory implies that some solution may be completely missed. Indeed, the nonlinear problem of an elastic rod loaded at its end is analogous to that of the nonlinear pendulum, considered as an example showing the Hamilton-Jacobi theory failing in providing all the solutions.
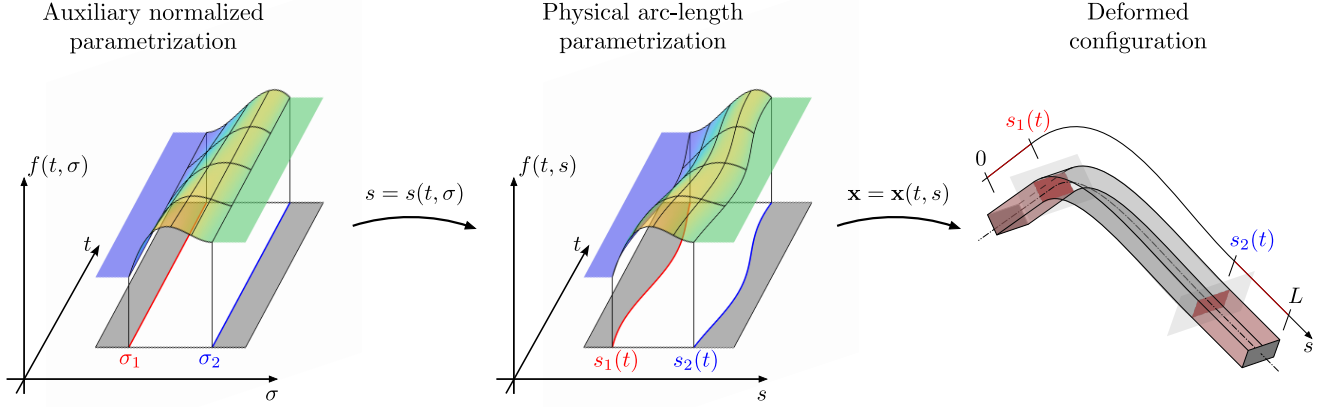
Figure 1: Auxiliary (left) and physical (right) spatial parametrizations of a one-dimensional structure having its flexible subdomain varying in time t (right). (Left) The auxiliary normalized parametrization within a time-constant domain through the space variable $\sigma \in [\sigma_1, \sigma_2]$. (Center) The physical arc-length parametrization within a time-varying domain through the space variable $s \in [s_1(t), s_2(t)]$. (Right) Deformed configuration of a one-dimensional structure of total length L, fully constrained to have null curvature within its end subdomains $s \in [0, s_1(t))$ and $s \in (s_2(t), L]$.

sliding-sleeve rod system with mass concentrated at the unconstrained tip [57], by considering quaternions to define the rotations of the cross-sections of the rod and dual numbers are used to obtain their final FE implementation. This methodology has been also enhanced in [58] to tackle the case of a rod with distributed mass interacting with one sliding-sleeve. The latter approach provides a robust ALE-FE framework for the most general case, however the dual numbers and the selection of quaternions for the kinematic parameters complicate the implementation, while the part of the rod constrained by the sleeve is simulated even though its kinematics can be directly assessed by the sliding-sleeve constraint. As a result, a lightweight ALE-FE implementation for the dynamic simulation of rods with distributed inertia and moving boundaries is not yet available.

To this purpose, inspired by the efficient dynamic FE model with fixed length developed by Bartels [59, 60] enhanced by the time integration algorithm by Papathanasiou [61], a FE model based on an ALE formulation is proposed for analyzing the planar dynamics of an inextensible and unshearable rod of finite length constrained at one or both ends by frictionless sliding sleeves, whose position and inclination can be varied in time. In this model the variable domain of the solution is defined through time-dependent configuration parameters, namely the arc-length coordinates of the exits of the sliding sleeves. These configuration parameters are a priori unknown and are modelled as degrees of freedom. The problem is formulated by splitting ab initio the rod into fully constrained and unconstrained segments, leading to the expression of the dynamics of the system solely by the fields defined on the variable domain corresponding to the unconstrained segment, and the configuration parameters. The underlying parametrization of the fields involved in the model is shown graphically in Fig. 1. For the ALE-FE model, the weak form of the governing equations is derived from the Hamiltonian principle using a variational approach, and then the integral equations complemented by the constraints are discretized in space leading to a system of ODEs, and subsequently the Newmark method is chosen to integrate the evolution in time. The source code of the developed software is made available [62].

The article is organized as follows. The nonlinear dynamics on variable domains is first discussed in detail together with an introduction to the ALE approach (Sect. 2), followed by the adaptation to the inextensible (and unshearable) sliding rod case (Sect. 3). Then, the derivation of the ALE-FE model is presented in Sect. 4. Finally, case studies and instability problems are investigated in Sect. 5, along with a comparison to previously published results, in order to showcase the robustness of the method in cases where instabilities lead to fast dynamics.

The proposed approach provides a powerful yet simple tool to analyze variable-domain mechanical systems for the design of reconfigurable structures for applications in soft actuation, energy harvesting and wave mitigation.

The present formulation is readily available for an extension to treat the three-dimensional dynamics of flexible one- and two-dimensional systems with varying domains.

2 Formulation of the nonlinear dynamics of one-dimensional structures with movable constraints

The general background theory for solving moving boundary problems is presented in this Section together with an introduction to the ALE approach in Sect. 2.2, adopted in the following for the numerical resolution. The mathematical foundation for addressing the nonlinear dynamics of one-dimensional structures with constraints movable along their domain and the general weak form of the governing equations can be obtained through the application of the Hamiltonian principle,

$$\int_{t_1}^{t_2} \delta\mathcal{L} \; \mathrm{d}t = 0, \qquad \forall \, t_1, t_2, \tag{1}$$

where $\mathcal{L}(t)$ is the Lagrangian of the structural system, being t the physical time.

In the presence of movable constraints, the whole domain can be partitioned in non-overlapping time-dependent subdomains, having the constraint as boundary condition. To this purpose, the one-dimensional domain $[0, L]$ (being L the domain size) for the space variable s is reparametrized by employing a bijective (1-1 and onto) map that depends on the configuration parameter vector $\mathbf{p} = \mathbf{p}(t)$. The variation of integral terms is treated through the Leibniz integral rule and finally material time derivatives are introduced in order to properly perform the integration by parts in time. This approach is analogous to Reynold's transport theorem in fluid mechanics, and yields a mathematical model for structural dynamics defined on arbitrary non-material frames of reference.

The introduced framework is exploited in Sect. 3 to analyze structures with variable domain as the result of the presence of sliding sleeves constraints. The latter splits the structure in two classes of variable subdomains differing in the type of imposed constraints, namely, a variable central subdomain $\mathcal{N}(\mathbf{p})$ with boundary conditions at its end points and two variable end subdomains $\mathcal{C}_1(\mathbf{p})$ and $\mathcal{C}_2(\mathbf{p})$, where the kinematics of the rod is fully constrained; see Fig. 1. These three subdomains are defined through the configuration parameters $s_1(\mathbf{p})$, and $s_2(\mathbf{p})$ describing the time-varying curvilinear coordinates along the rod where the sliding sleeves exit point is located,

$$\mathcal{N}(\mathbf{p}) := [s_1(\mathbf{p}), s_2(\mathbf{p})], \quad \mathcal{C}_1(\mathbf{p}) := [0, s_1(\mathbf{p})), \quad \mathcal{C}_2(\mathbf{p}) := (s_2(\mathbf{p}), L]. \tag{2}$$

The two classes of variable subdomains requires a different treatment. In particular, subdomain $\mathcal{N}$ is governed by two equations, one for the kinematic fields and one for the configuration parameter vector $\mathbf{p}(t)$, while subdomains $\mathcal{C}_1$ and $\mathcal{C}_2$ are respectively governed by one equation only for $\mathbf{p}(t)$. This particular feature of the latter subdomains is due to the description of all kinematic fields through $\mathbf{p}(t)$, meaning that the Lagrangian of the fully constrained parts of the rod can be expressed explicitly as a function of $\mathbf{p}(t)$ and its time derivatives. It is noted that the dynamics of the kinematically constrained parts ($\mathcal{C}_1$ and $\mathcal{C}_2$) is trivial in the sense that it depends only on the configurational parameter vector $\mathbf{p}(t)$. Therefore, their contribution in the equations of motion can be evaluated a-priori and expressed as time-dependent concentrated loads at the moving ends, corresponding to the two sliding sleeve exits.

In the remainder of this Section, the only variation that will be evaluated is the first variation $\delta\mathcal{L}$ of the Lagrangian $\mathcal{L}$, which is the only one relevant to the dynamic problem formulation.

2.1 First variation on non-material domains

Following partition (2), the Lagrangian of the structural system can be evaluated as the sum of the Lagrangians $\mathcal{L}_\mathcal{N}$, $\mathcal{L}_{\mathcal{C}_1}$, and $\mathcal{L}_{\mathcal{C}_2}$ respectively associated with variable subdomains $\mathcal{N}(\mathbf{p})$, $\mathcal{C}_1(\mathbf{p})$, and $\mathcal{C}_2(\mathbf{p})$,

$$\mathcal{L} = \mathcal{L}_\mathcal{N} + \mathcal{L}_{\mathcal{C}_1} + \mathcal{L}_{\mathcal{C}_2}. \tag{3}$$

The Lagrangian $\mathcal{L}_\mathcal{N}$ depends on the fields along $\mathcal{N}$ and terms involving evaluation of these fields at specific discrete points, while $\mathcal{L}_{\mathcal{C}_1}$ and $\mathcal{L}_{\mathcal{C}_2}$ are dependent only on $\mathbf{p}(t)$,

$$\mathcal{L}_\mathcal{N}(t, \boldsymbol{\xi}, \dot{\boldsymbol{\xi}}; \mathbf{p}, \dot{\mathbf{p}}) = \int_{s_1(\mathbf{p})}^{s_2(\mathbf{p})} \mathcal{F}(t, \boldsymbol{\xi}, \dot{\boldsymbol{\xi}}; \mathbf{p}, \dot{\mathbf{p}}) \; \mathrm{d}s + \mathcal{B}_\mathcal{N}(t, \boldsymbol{\xi}_1^*, \dots, \boldsymbol{\xi}_Q^*), \qquad \mathcal{L}_{\mathcal{C}_i}(\mathbf{p}, \dot{\mathbf{p}}) = \mathcal{B}_{\mathcal{C}_i}(\mathbf{p}, \dot{\mathbf{p}}), \quad i = 1, 2, \tag{4}$$

where a superimposed dot represents the partial derivative in the time t (defined on a *material* point), $\mathcal{F}$ is a function of the fields involved in the problem, collected in the vector $\boldsymbol{\xi} = \boldsymbol{\xi}(t, s)$ along with their space derivatives, that defines the system configuration and whose integration has limits that are functions of the configuration parameters $\mathbf{p}$. Moreover, $\mathcal{B}_{\mathcal{C}_i}$ $(i = 1, 2)$ are functions of $\mathbf{p}$, while $\mathcal{B}_{\mathcal{N}}$ is a function of $\boldsymbol{\xi}_q^* = \boldsymbol{\xi}(s_q^*)$ evaluated at Q specific points $s_q^*(t, \mathbf{p}) \in [s_1, s_2]$, such as points of concentrated force application and of constraint location (the latter with the meaning of Lagrangian multipliers imposing kinematic boundary conditions). The quantities $\mathbf{p}$ and $\dot{\mathbf{p}}$ appearing after the semicolon in the argument list of the above functional $\mathcal{L}$ and function $\mathcal{F}$ represent parameters on which these are implicitly dependent only. Next, summing up all the terms, the functional $\mathcal{L}$, parametrized in space by the curvilinear coordinate s within the time-varying compact domain $(s_1(\mathbf{p}), s_2(\mathbf{p}))$ can be generally defined as

$$\mathcal{L}(t, \boldsymbol{\xi}, \dot{\boldsymbol{\xi}}; \mathbf{p}, \dot{\mathbf{p}}) = \int_{s_1(\mathbf{p})}^{s_2(\mathbf{p})} \mathcal{F}(t, \boldsymbol{\xi}, \dot{\boldsymbol{\xi}}; \mathbf{p}, \dot{\mathbf{p}}) \, \mathrm{d}s + \mathcal{B}(t, \boldsymbol{\xi}_1^*, \ldots, \boldsymbol{\xi}_Q^*, \mathbf{p}, \dot{\mathbf{p}}), \tag{5}$$

where $\mathcal{B} = \mathcal{B}_{\mathcal{N}} + \mathcal{B}_{\mathcal{C}_1} + \mathcal{B}_{\mathcal{C}_2}$.

The variation $\delta\mathcal{L}$ of the functional $\mathcal{L}$, Eq. (5), can be evaluated as

$$\delta\mathcal{L} = \delta_{\boldsymbol{\xi}}\mathcal{L} + \delta_{\dot{\boldsymbol{\xi}}}\mathcal{L} + \delta_{\mathbf{p}}\mathcal{L} + \delta_{\dot{\mathbf{p}}}\mathcal{L}, \tag{6}$$

where $\delta_{\boldsymbol{\xi}}\mathcal{L}$, $\delta_{\dot{\boldsymbol{\xi}}}\mathcal{L}$, $\delta_{\mathbf{p}}\mathcal{L}$, and $\delta_{\dot{\mathbf{p}}}\mathcal{L}$ are variations of the functional $\mathcal{L}$ with respect to the single corresponding variable, namely

$$\delta_{\mathbf{z}}(\cdot) = (\cdot)_{,\mathbf{z}} \cdot \delta\mathbf{z}, \tag{7}$$

where the notation $(\cdot)_{,\mathbf{z}}$ is introduced to denote the partial derivative of a quantity with respect to a variable $\mathbf{z}$; i.e. $(\cdot)_{,\mathbf{z}} = \partial(\cdot)/\partial\mathbf{z}$.

Considering the introduced assumptions about the functionals, Eq. (4), the following derivatives vanish

$$\mathcal{F}_{,\mathbf{p}} = \mathcal{F}_{,\dot{\mathbf{p}}} = \mathcal{B}_{\mathcal{N},\mathbf{p}} = \mathcal{B}_{\mathcal{N},\dot{\mathbf{p}}} = \mathbf{0}, \qquad \mathcal{B}_{\mathcal{C}_i,\boldsymbol{\xi}_q^*} = \mathbf{0}, \quad i = 1, 2, \qquad q = 1, \ldots, Q, \tag{8}$$

and, by using the Leibniz integral rule and the chain rule, the variations $\delta_{\boldsymbol{\xi}}\mathcal{L}$, $\delta_{\dot{\boldsymbol{\xi}}}\mathcal{L}$, $\delta_{\mathbf{p}}\mathcal{L}$, and $\delta_{\dot{\mathbf{p}}}\mathcal{L}$ reduce to

$$\delta_{\boldsymbol{\xi}}\mathcal{L} = \int_{s_1(\mathbf{p})}^{s_2(\mathbf{p})} \mathcal{F}_{,\boldsymbol{\xi}} \cdot \delta\boldsymbol{\xi} \, \mathrm{d}s + \sum_{q=1}^{Q} \mathcal{B}_{,\boldsymbol{\xi}_q^*} \cdot \delta\boldsymbol{\xi}_q^*, \qquad\qquad \delta_{\dot{\boldsymbol{\xi}}}\mathcal{L} = \int_{s_1(\mathbf{p})}^{s_2(\mathbf{p})} \mathcal{F}_{,\dot{\boldsymbol{\xi}}} \cdot \delta\dot{\boldsymbol{\xi}} \, \mathrm{d}s,$$

$$\delta_{\mathbf{p}}\mathcal{L} = \left\{ \left[\mathcal{F} \, s_{,\mathbf{p}} \right]_{s_1}^{s_2} + \mathcal{B}_{,\mathbf{p}} + \sum_{q=1}^{Q} \mathcal{B}_{,\boldsymbol{\xi}_q^*} \cdot \boldsymbol{\xi}_{q,s_q^*}^* \, s_{q,\mathbf{p}}^* \right\} \cdot \delta\mathbf{p}, \qquad \delta_{\dot{\mathbf{p}}}\mathcal{L} = \mathcal{B}_{,\dot{\mathbf{p}}} \cdot \delta\dot{\mathbf{p}}, \tag{9}$$

so that the first variation $\delta\mathcal{L}$ results to

$$\delta\mathcal{L} = \underbrace{\int_{s_1(\mathbf{p})}^{s_2(\mathbf{p})} \left(\mathcal{F}_{,\boldsymbol{\xi}} \cdot \delta\boldsymbol{\xi} + \mathcal{F}_{,\dot{\boldsymbol{\xi}}} \cdot \delta\dot{\boldsymbol{\xi}} \right) \mathrm{d}s + \sum_{q=1}^{Q} \mathcal{B}_{,\boldsymbol{\xi}_q^*} \cdot \delta\boldsymbol{\xi}_q^*}_{\text{'fixed domain' terms}} + \underbrace{\left\{ \left[\mathcal{F} \, s_{,\mathbf{p}} \right]_{s_1}^{s_2} + \mathcal{B}_{,\mathbf{p}} + \sum_{q=1}^{Q} \mathcal{B}_{,\boldsymbol{\xi}_q^*} \cdot \boldsymbol{\xi}_{q,s_q^*}^* \, s_{q,\mathbf{p}}^* \right\} \cdot \delta\mathbf{p} + \mathcal{B}_{,\dot{\mathbf{p}}} \cdot \delta\dot{\mathbf{p}}}_{\text{configuration parameter-dependent terms}}.$$

$$\tag{10}$$

It is finally noted that the following identities relevant to the evaluation of the derivatives of $\delta\mathcal{B}$ hold

$$\mathcal{B}_{,\boldsymbol{\xi}_q^*} = \mathcal{B}_{\mathcal{N},\boldsymbol{\xi}_q^*}, \qquad \mathcal{B}_{,\mathbf{p}} = \mathcal{B}_{\mathcal{C}_1,\mathbf{p}} + \mathcal{B}_{\mathcal{C}_2,\mathbf{p}}, \qquad \mathcal{B}_{,\dot{\mathbf{p}}} = \mathcal{B}_{\mathcal{C}_1,\dot{\mathbf{p}}} + \mathcal{B}_{\mathcal{C}_2,\dot{\mathbf{p}}}, \tag{11}$$

which can be obtained by considering the expressions in Eq. (4) for $\mathcal{B}_{\mathcal{N}}$, $\mathcal{B}_{\mathcal{C}_1}$, and $\mathcal{B}_{\mathcal{C}_2}$.

2.2 Reparametrization to a time-independent 'auxiliary' domain

The first variation $\delta\mathcal{L}$, Eq. (10), involved in the Hamiltonian principle (1) contains time derivative variations $\delta\dot{\boldsymbol{\xi}}$ and $\delta\dot{\mathbf{p}}$, which need to be treated for obtaining the weak form of the governing equations. Although standard for time-independent domains, their integration by parts for time-dependent domains requires special attention.

More specifically, following the ALE approach, the spatial integral has to be transformed to a time-independent 'auxiliary' domain, to allow the change in the integration order between time and space. For this reason, a diffeomorphic map is defined such that a non-varying compact domain for the 'auxiliary' spatial variable σ is mapped into a varying domain for the 'physical' spatial variable s,

and without loss of generality and for simplicity, the following linear relation is adopted

$$s(t, \sigma) = s_1(t) + (s_2(t) - s_1(t)) \, \sigma, \tag{12}$$

which maps $\sigma \in [0, 1]$ onto $s \in [s_1(t), s_2(t)]$. As a consequence, after integration by parts of the terms containing time-derivatives of variations, the Hamiltonian principle (1) for variable domains can be rewritten as

$$\left[\int_{s_1}^{s_2} \mathcal{F}_{,\dot{\boldsymbol{\xi}}} \cdot \delta\boldsymbol{\xi} \, \mathrm{d}s \right]_{t_1}^{t_2} - \int_{t_1}^{t_2} \int_{s_1}^{s_2} \left\{ \left[\frac{\mathrm{D}}{\mathrm{D}t} \mathcal{F}_{,\dot{\boldsymbol{\xi}}} + j' \, \mathcal{F}_{,\dot{\boldsymbol{\xi}}} - \mathcal{F}_{,\boldsymbol{\xi}} \right] \cdot \delta\boldsymbol{\xi} + \dot{s} \, \mathcal{F}_{,\dot{\boldsymbol{\xi}}} \cdot \delta\boldsymbol{\xi}_{,s} \right\} \mathrm{d}s \, \mathrm{d}t + \int_{t_1}^{t_2} \left[\mathcal{F} \, s_{,\mathbf{p}} \right]_{s_1}^{s_2} \cdot \delta\mathbf{p} \, \mathrm{d}t$$

$$+ \left[\mathcal{B}_{,\dot{\mathbf{p}}} \cdot \delta\mathbf{p} \right]_{t_1}^{t_2} + \int_{t_1}^{t_2} \left\{ \sum_{q=1}^{Q} \mathcal{B}_{,\boldsymbol{\xi}_q^*} \cdot \delta\boldsymbol{\xi}_q^* + \left[\sum_{q=1}^{Q} \mathcal{B}_{,\boldsymbol{\xi}_q^*} \cdot \boldsymbol{\xi}_{q,s}^* \, s_{q,\mathbf{p}}^* + \mathcal{B}_{,\mathbf{p}} - (\mathcal{B}_{,\dot{\mathbf{p}}})_{,t} \right] \cdot \delta\mathbf{p} \right\} \mathrm{d}t = 0, \tag{13}$$

where $j(t)$ and $\mathrm{D}(\cdot)/\mathrm{D}t$ respectively denote the transformation Jacobian and the *material* time derivative operator,

$$j(t) = s_{,\sigma}(s), \quad \frac{\mathrm{D}(\cdot)}{\mathrm{D}t} = (\cdot)_{,t} + (\cdot)_{,s} \, \dot{s}, \tag{14}$$

while $j^{-1}(t)$ is the inverse of the transformation Jacobian and j' denotes the gradient of the time derivative of the transformation Jacobian

$$j^{-1}(t) = \sigma_{,s}(t), \quad j' = (j)^{\cdot} \cdot j^{-1}, \tag{15}$$

which, by considering the adopted linear mapping (12), reduces to

$$j^{-1}(t) = \frac{1}{j(t)}, \quad j' = (s_{,t})_{,s}. \tag{16}$$

Since the Hamiltonian principle (13) holds for every admissible variations $\delta\boldsymbol{\xi}$, and $\delta\mathbf{p}$, that satisfies

$$\delta\boldsymbol{\xi}(t) = \delta\mathbf{p}(t) = \mathbf{0}, \quad \text{for } t = t_1, t_2, \tag{17}$$

the weak form of the governing equations follows as the following differential system

$$\begin{cases} \int_{s_1}^{s_2} \left[\left(\frac{\mathrm{D}}{\mathrm{D}t} \mathcal{F}_{,\dot{\boldsymbol{\xi}}} + j' \, \mathcal{F}_{,\dot{\boldsymbol{\xi}}} - \mathcal{F}_{,\boldsymbol{\xi}} \right) \cdot \delta\boldsymbol{\xi} + \dot{s} \, \mathcal{F}_{,\dot{\boldsymbol{\xi}}} \cdot \delta\boldsymbol{\xi}_{,s} \right] \mathrm{d}s - \sum_{q=1}^{Q} \mathcal{B}_{,\boldsymbol{\xi}_q^*} \cdot \delta\boldsymbol{\xi}_q^* = 0, \\[4mm] \left[\left(\mathcal{F} \, s_{,\mathbf{p}} \right) \Big|_{s_1}^{s_2} + \sum_{q=1}^{Q} \mathcal{B}_{,\boldsymbol{\xi}_q^*} \cdot \boldsymbol{\xi}_{q,s}^* \, s_{q,\mathbf{p}}^* + \mathcal{B}_{,\mathbf{p}} - (\mathcal{B}_{,\dot{\mathbf{p}}})_{,t} \right] \cdot \delta\mathbf{p} = 0. \end{cases} \tag{18}$$

It can be noted that the governing equations (18) represent a system of one partial differential equation and one ordinary differential equation, where the latter expresses interface conditions at the moving boundaries s_1 and s_2. It is finally noted that the equations of motion can also be independently obtained through dynamic equilibrium by considering the presence of a configurational force expressed by an outward nonlinear tangential reaction force at each frictionless sliding sleeve exit.

3 Structural dynamics of inextensible geometrically nonlinear rods with ends constrained by sliding sleeves

The planar nonlinear dynamics of a rod constrained at its two edges by sliding sleeves is introduced by using the framework established in Sect. 2. The rod, of uniform bending stiffness B and linear mass density γ, is modelled
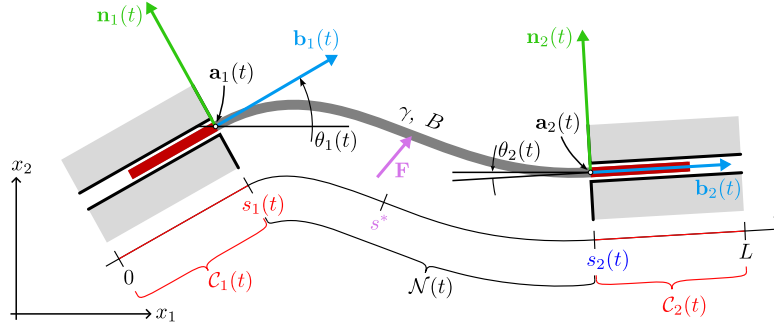
Figure 2: Sketch of the planar structural system with an unconstrained time-varying domain $\mathcal{N}(t)$. The one-dimensional structure is constrained at its ends by two independent sliding sleeves controlled in the time t through the position vector $\mathbf{p}_i(t)$ and the unit tangent $\mathbf{b}_i(t)$, the latter inclined by the angle $\theta_i(t)$ (positive when counter-clockwise) with respect to the x_1 axis ($i = 1, 2$). The rod has linear mass density γ, total length L and is flexible under a bending stiffness B, but inextensible and unshearable. The position of the sliding sleeves exit along the rod is measured through the curvilinear coordinate $s_1(t)$ and $s_2(t)$, whose in turn define the fully-constrained time-varying subdomains $\mathcal{C}_1(t)$ and $\mathcal{C}_2(t)$.

as inextensible, meaning that it displays null axial strain, and unshearable, meaning that the cross sections remain orthogonal to the rod's axis. The straight configuration is considered as the unloaded state for the rod. The cross section along the rod is identified through the curvilinear coordinate $s \in [0, L]$, being L the total length.

The case of rods constrained by sliding sleeves at both ends is analyzed first, while the case of only one side constrained by a sliding sleeve and the other free is then obtained as a simplification.

3.1 Rod constrained at each of its edges by two independent sliding sleeves

Following Sect. 2, the curvilinear coordinate domain, $s \in [0, L]$, can be split in three variable subdomains, two associated with the rod's portions fully constrained by the sliding sleeves (see Fig. 2), named $\mathcal{C}_1(t)$ and $\mathcal{C}_2(t)$, and one associated with the unconstrained rod's portion, $\mathcal{N}(t)$, Eq. (2) with $s_1(t)$ and $s_2(t)$ as configuration parameters,

$$\mathcal{C}_1(t) = [0, s_1(t)], \quad \mathcal{C}_2(t) = [s_2(t), L], \quad \mathcal{N}(t) = [s_1(t), s_2(t)]. \tag{19}$$

The presence of a (constant) gravitational distributed force $\gamma\mathbf{g}$ along the entire rod and of concentrated external forces $\mathbf{F}_q(t)$ at Q curvilinear coordinates $s_q^*(t, \mathbf{p})$ is considered ($q = 1, .., Q$).

The position in time t of a material point along the rod, associated with the curvilinear coordinate s, is described by the vector $\mathbf{x}(t, s)$ collecting the two coordinates in the Cartesian x_1–x_2 reference system. The inextensibility constraint dictates that the spatial derivative of $\mathbf{x}$, corresponding to a tangent vector to the rod axis, has a unit modulus at every material point, namely

$$||\mathbf{x}_{,s}(t, s)|| = 1, \qquad \forall s \in [0, L], \tag{20}$$

where $|| \cdot ||$ represents the Euclidean norm.

Moreover, the position $\mathbf{x}(t, s)$ of material points of the rod inside the two sliding sleeves is constrained by (repeated index is not summed)

$$\mathbf{x}(t, s) = \mathbf{a}_i(t) + [s - s_i(t)] \ \mathbf{b}_i(t), \quad s \in \mathcal{C}_i(t), \quad i = 1, 2, \tag{21}$$

where $\mathbf{a}_1(t)$ and $\mathbf{a}_2(t)$ are the positions of the exit of the two sliding sleeves, while $\mathbf{b}_1(t)$, and $\mathbf{b}_2(t)$ are the unit vectors parallel to the sliding-sleeves, according to the direction of the rod's tangent, inclined at angles θ_1 and θ_2 (positive angle when counterclockwise) with respect to the x_1 axis , Fig. 2, namely

$$\mathbf{b}_i(t) = \begin{pmatrix} \cos\theta_i(t) \\ \sin\theta_i(t) \end{pmatrix}. \tag{22}$$

From the constrained position fields (21), the fields of material velocity $\dot{\mathbf{x}}(t,s)$ and acceleration $\ddot{\mathbf{x}}(t,s)$ are given in the fully constrained subdomains $\mathcal{C}_1$ and $\mathcal{C}_2$ by

$$\begin{aligned}
\dot{\mathbf{x}}(t,s) &= \dot{\mathbf{a}}_i(t) - \dot{s}_i(t)\,\mathbf{b}_i(t) + [s - s_i(t)]\,\dot{\mathbf{b}}_i(t), \\
\ddot{\mathbf{x}}(t,s) &= \ddot{\mathbf{a}}_i(t) - \ddot{s}_i(t)\,\mathbf{b}_i(t) - 2\,\dot{s}_i(t)\,\dot{\mathbf{b}}_i(t) + [s - s_i(t)]\,\ddot{\mathbf{b}}_i(t),
\end{aligned} \qquad s \in \mathcal{C}_i(t), \quad i = 1,2. \tag{23}$$

From Eq. (21), the continuity along the rod of both the position $\mathbf{x}(t,s)$ and the tangent $\mathbf{x}_{,s}$ leads the two following additional constraints at each sliding sleeve

$$\mathbf{x}\left(t, s_i(t)\right) - \mathbf{a}_i(t) = \mathbf{0}, \quad \mathbf{x}_{,s}(t, s_i(t)) \cdot \mathbf{n}_i(t) = 0, \quad i = 1,2, \tag{24}$$

where the unit vector $\mathbf{n}_i(t)$ is the normal to the i-th sliding sleeve, namely

$$\mathbf{n}_i(t) = \begin{pmatrix} -\sin\theta_i(t) \\ \cos\theta_i(t) \end{pmatrix}. \tag{25}$$

The kinetic energy $\mathcal{T}_{Ci}$ and the total potential energy $\mathcal{V}_{Ci}$ associated to the rod portion inside the i-th sliding sleeve (subdomain $\mathcal{C}_i$) are given by

$$\mathcal{T}_{Ci} = \frac{\gamma}{2} \int_{\mathcal{C}_i(t)} \dot{\mathbf{x}}^2(t,s)\,\mathrm{d}s, \quad \mathcal{V}_{Ci} = -\gamma\,\mathbf{g} \cdot \int_{\mathcal{C}_i(t)} \mathbf{x}(t,s)\,\mathrm{d}s, \quad i = 1,2. \tag{26}$$

The kinetic $\mathcal{T}_{Ci}\left(s_i(t), \dot{s}_i(t)\right)$ and potential energy $\mathcal{V}_{Ci}\left(s_i(t)\right)$ ($i = 1,2$) can be evaluated by substituting the expressions for the rod position $\mathbf{x}(t,s)$ and velocity $\dot{\mathbf{x}}(t,s)$, Eqs. (21) and (23)$_1$, as functions only of the configuration parameters $s_1(t)$ and $s_2(t)$ and their velocity $\dot{s}_1(t)$ and $\dot{s}_2(t)$ as follows (δ_{ij} is the Kronecker delta, repeated index is not summed)

$$\begin{aligned}
\mathcal{T}_{Ci}(t) = \quad & \frac{\gamma}{2} \left\{ \left[(\dot{\mathbf{a}}_i - \dot{s}_i \mathbf{b}_i)^2 - 2\,s_i\,\dot{\mathbf{a}}_i \cdot \dot{\mathbf{b}}_i + 2\,s_i\,\dot{s}_i\,\mathbf{b}_i \cdot \dot{\mathbf{b}}_i + s_i^2\,\dot{\mathbf{b}}_i^2 \right] \left(\delta_{2i} L - (-1)^i\,s_i \right) \right. \\
& \left. + \left[\dot{\mathbf{a}}_i \cdot \dot{\mathbf{b}}_i - \dot{s}_i\,\mathbf{b}_i \cdot \dot{\mathbf{b}}_i - s_i\,\dot{\mathbf{b}}_i^2 \right] \left(\delta_{2i} L^2 - (-1)^i\,s_i^2 \right) + \frac{\dot{\mathbf{b}}_i^2}{3} \left(\delta_{2i} L^3 - (-1)^i\,s_i^3 \right) \right\}, \qquad i = 1,2. \tag{27} \\
\mathcal{V}_{Ci}(t) = \quad & -\gamma\mathbf{g} \cdot \left[(\mathbf{a}_i - s_i\,\mathbf{b}_i) \left(\delta_{2i} L - (-1)^i\,s_i \right) + \frac{\mathbf{b}_i}{2} \left(\delta_{2i} L^2 - (-1)^i\,s_i^2 \right) \right],
\end{aligned}$$

The kinetic $\mathcal{T}_\mathcal{N}\left(s_1(t), s_2(t), \dot{\mathbf{x}}(t,s)\right)$ and the potential $\mathcal{V}_\mathcal{N}\left(s_1(t), s_2(t), \mathbf{x}(t,s)\right)$ energies of the central portion of the rod $\mathcal{N}$ are given by

$$\mathcal{T}_\mathcal{N} = \frac{\gamma}{2} \int_{s_1(t)}^{s_2(t)} \dot{\mathbf{x}}^2(t,s)\,\mathrm{d}s, \qquad \mathcal{V}_\mathcal{N} = \frac{B}{2} \int_{s_1(t)}^{s_2(t)} \mathbf{x}_{,ss}^2(t,s)\,\mathrm{d}s - \gamma\,\mathbf{g} \cdot \int_{s_1(t)}^{s_2(t)} \mathbf{x}(t,s)\,\mathrm{d}s - \sum_q^Q \mathbf{F}_q(t) \cdot \mathbf{x}(t, s_q^*). \tag{28}$$

The Lagrangian $\mathcal{L}$ of the whole system is provided by

$$\begin{aligned}
\mathcal{L} = \, & \mathcal{T}_\mathcal{N} + \mathcal{T}_{\mathcal{C}_1} + \mathcal{T}_{\mathcal{C}_2} - \mathcal{V}_\mathcal{N} - \mathcal{V}_{\mathcal{C}_1} - \mathcal{V}_{\mathcal{C}_2} \\
& - \int_{s_1}^{s_2} \frac{N}{2} \left(\mathbf{x}_{,s}^2 - 1 \right) \mathrm{d}s - \mathbf{R}_1 \cdot [\mathbf{x}(s_1) - \mathbf{a}_1] - M_1\,\mathbf{n}_1 \cdot \mathbf{x}_{,s}(s_1) - \mathbf{R}_2 \cdot [\mathbf{x}(s_2) - \mathbf{a}_2] - M_2\,\mathbf{n}_2 \cdot \mathbf{x}_{,s}(s_2),
\end{aligned} \tag{29}$$

where $N(t,s)$ is a Lagrange multiplier field associated with the inextensibility constraint defined on $(s_1(t), s_2(t))$, and $\mathbf{R}_1(t)$, $\mathbf{R}_2(t)$, $M_1(t)$, and $M_2(t)$ are Lagrange multipliers associated with the continuity of the rod at the sliding sleeve exits. These Lagrangian multipliers have the physical meaning of internal axial force ($N(t,s)$) along the central portion of the rod and of the balancing reaction force vector ($\mathbf{R}_i(t)$) and moment ($M_i(t)$) at the i-th sliding sleeve exit respectively. It is noted that, as shown at the end of this SubSection, the force $\mathbf{R}_i$ has to not be confused with the concentrated reaction $\mathbf{C}_i$ realized at the i-th sliding sleeve exit.

Finally, given the Lagrangian $\mathcal{L}$ (29), the following weak form of the governing equations of the structural system can be obtained from Eq. (18) as

$$
\int_{s_1(t)}^{s_2(t)} \left\{ \gamma \left[\frac{\mathrm{D}^2\mathbf{x}}{\mathrm{D}t^2} - \ddot{s}\,\mathbf{x}_{,s} + j'\,\frac{\mathrm{D}\mathbf{x}}{\mathrm{D}t} - \dot{s}\left(\frac{\mathrm{D}\mathbf{x}}{\mathrm{D}t}\right)_{,s} - \mathbf{g} \right] \cdot \delta\mathbf{x} \right.
$$

$$
+ \left[\gamma\,\dot{s}\left(\frac{\mathrm{D}\mathbf{x}}{\mathrm{D}t} - \dot{s}\,\mathbf{x}_{,s}\right) + N\,\mathbf{x}_{,s} \right] \cdot \delta\mathbf{x}_{,s} + B\,\mathbf{x}_{,ss} \cdot \delta\mathbf{x}_{,ss} \Bigg\}\,\mathrm{d}s
$$

$$
\left. - \sum_{q}^{Q} \mathbf{F}_q(t) \cdot \delta\mathbf{x}(t, s_q^*) + \sum_{i=1}^{2} \left[\mathbf{R}_i \cdot \delta\mathbf{x}(s_i) + M_i\,\mathbf{n}_i \cdot \delta\mathbf{x}_{,s}(s_i) \right] = 0, \right. \tag{30}
$$

$$
\left\{ \left(\frac{\gamma}{2}\dot{\mathbf{x}}^2(s_i) - \frac{B}{2}\mathbf{x}_{,ss}^2(s_i) + \gamma\mathbf{g}\cdot\mathbf{x}(s_i) \right)(-1)^i + \mathcal{T}_{Ci,s_i} - (\mathcal{T}_{Ci,\dot{s}_i})_{,t} - \mathcal{V}_{Ci,s_i} + (\mathcal{V}_{Ci,\dot{s}_i})_{,t} \right.
$$

$$
\left. - \mathbf{R}_i \cdot \mathbf{x}_{,s}(s_i) - M_i\,\mathbf{n}_i \cdot \mathbf{x}_{,ss}(s_i) \right\}\delta s_i = 0, \quad i = 1, 2,
$$

where the identity

$$
\frac{\mathrm{D}\dot{\mathbf{x}}}{\mathrm{D}t} = \frac{\mathrm{D}^2\mathbf{x}}{\mathrm{D}t^2} - \ddot{s}\,\mathbf{x}_{,s} - \dot{s}\left(\frac{D\mathbf{x}}{Dt}\right)_{,s} + \dot{s}\,j'\,\mathbf{x}_{,s}, \tag{31}
$$

has been used in order to express the weak form using quantities defined on the moving mesh and the function values at s_i should be interpreted as the evaluation at s_1^+ for $i = 1$ (at s_2^- for $i = 2$), providing the function value at the coordinate s_1 (s_2) approaching from the right (left). The weak form (30) of the governing equations is complemented by the following algebraic constraints

$$
\int_{s_1(t)}^{s_2(t)} \frac{1}{2}\,\delta N\,(\mathbf{x}_{,s} \cdot \mathbf{x}_{,s} - 1)\,\mathrm{d}s = 0, \quad \delta\mathbf{R}_1 \cdot (\mathbf{x}(t, s_1) - \mathbf{a}_1(t)) = 0, \quad \delta\mathbf{R}_2 \cdot (\mathbf{x}(t, s_2) - \mathbf{a}_2(t)) = 0,
$$

$$
\delta M_1\,\mathbf{n}_1(t) \cdot \mathbf{x}_{,s}(t, s_1) = 0, \qquad\qquad \delta M_2\,\mathbf{n}_2(t) \cdot \mathbf{x}_{,s}(t, s_2) = 0. \tag{32}
$$

It is noted here that in addition to the admissibility conditions (17) the variations $\delta\mathbf{x}$ need to satisfy also the inextensibility condition

$$
\delta\mathbf{x}_{,s}(t, s) \cdot \mathbf{x}_s(t, s) = 0, \quad \forall t, \quad \forall s \in \mathcal{N}(t). \tag{33}
$$

Strong form. Assuming B constant, sufficient regularity for $\mathbf{x}$ and N, and using integration by parts for the terms of Eq. (30)$_1$ involving space derivatives of the variations $\delta\mathbf{x}$, the problem can be strongly formulated in the non-material frame of reference as

$$
\gamma\left[\frac{\mathrm{D}\dot{\mathbf{x}}}{\mathrm{D}t} - \dot{s}\cdot\left(\frac{\mathrm{D}\mathbf{x}}{\mathrm{D}t}\right)_{,s} \right] + (\gamma\dot{s}\dot{s}_{,s} - N_{,s})\,\mathbf{x}_{,s} + (\gamma\dot{s}^2 - N)\,\mathbf{x}_{,ss} + B\,\mathbf{x}_{,ssss} - \gamma\,\mathbf{g} = 0, \quad \forall\, s = s(t, \sigma),\ t, \tag{34}
$$

or, equivalently, in the material framework as

$$
B\,\mathbf{x}_{,ssss} - (N\,\mathbf{x}_{,s})_{,s} = \gamma\,(\mathbf{g} - \ddot{\mathbf{x}}), \quad \forall\, s,\, t, \tag{35}
$$

complemented by the natural boundary conditions

$$
\mathbf{R}_1 - \left[\gamma\,\dot{s}\,\dot{\mathbf{x}} + N\,\mathbf{x}_{,s} - B\,\mathbf{x}_{,sss} \right]_{s_1^+} = \mathbf{0}, \qquad M_1\,\mathbf{n}_1 - B\,\mathbf{x}_{,ss}(s_1^+) = \mathbf{0},
$$

$$
\mathbf{R}_2 + \left[\gamma\,\dot{s}\,\dot{\mathbf{x}} + N\,\mathbf{x}_{,s} - B\,\mathbf{x}_{,sss} \right]_{s_2^-} = \mathbf{0}, \qquad M_2\,\mathbf{n}_2 - B\,\mathbf{x}_{,ss}(s_2^-) = \mathbf{0}, \tag{36}
$$

in addition to Eq. (30)$_2$ and under the inextensibility constraint, Eq. (20).

Eqs. $(30)_2$ and (36) allow to write the transverse and sliding component of the forces $\mathbf{R}_i$ $(i = 1, 2)$ as

$$\mathbf{R}_i \cdot \mathbf{n}_i = (-1)^i B\, \mathbf{x}_{,sss}(s_i) \cdot \mathbf{n}_i, \qquad \mathbf{R}_i \cdot \mathbf{b}_i = (-1)^i \frac{M_i^2}{2\,B} + T_i, \tag{37}$$

where T_i models the sliding forces developed due to the motion of the rod's portion fully constrained by the i-th sliding sleeve and is a function of the vectors $\mathbf{a}_i$, and $\mathbf{b}_i$ $(i = 1, 2)$

$$T_i = T_i(\mathbf{a}_i, \dot{\mathbf{a}}_i, \ddot{\mathbf{a}}_i, \mathbf{b}_i, \dot{\mathbf{b}}_i, \ddot{\mathbf{b}}_i) = \mathcal{T}_{Ci,s_i} - (\mathcal{T}_{Ci,\dot{s}_i})_{,t} - \mathcal{V}_{Ci,s_i} + (-1)^i \gamma \left(\frac{\dot{s}_1^2}{2} + \mathbf{g} \cdot \mathbf{a}_i \right). \tag{38}$$

Therefore, $\mathbf{R}_i$ balances the sum of the concentrated force $\mathbf{C}_i$ at the i-th sliding sleeve exit, as obtained in [56], and the additional sliding force T_i developed at the constrained segments of the rod due to the motion of the sleeves,

$$\mathbf{R}_i = -\mathbf{C}_i + T_i \mathbf{b}_i. \tag{39}$$

The strong form of the equations of motion, along with the boundary conditions and the relation between $\mathbf{R}_i$ and M_i, Eq. (37), are consistent with the derivation reported by Armanini et al. [56], as evident from a comparison of Eq. (35), and (37) with Eq. (15), and Eq. (27) in [56] respectively.

It is noted that although Eq. (35) is representative of a conservative system, the expression of the system in a non-material frame entails the contribution of advection terms. Therefore, since the weak form of the ALE formulation is used to obtain the numerical model in Sect. 4, it is expected that the conservation of energy may be violated when a standard time-stepping algorithm is used. To this purpose, special attention has to be paid to the time integration method for the numerical implementation of the model, as disclosed in Sect. 4.

3.2 Rod constrained by a sliding sleeve at one end only

The case where the rod is constrained by only one sliding sleeve can be obtained by setting $s_2 = L$, $\mathbf{R}_2 = 0$, and $M_2 = 0$. It follows also that the variation δs_2 vanishes and therefore Eq. $(30)_2$ with $i = 2$ becomes trivial, allowing for the reduction of the remaining ones as

$$\int_{s_1(t)}^{L} \left\{ \gamma \left[\frac{\mathrm{D}^2 \mathbf{x}}{\mathrm{D} t^2} - \ddot{s}\, \mathbf{x}_{,s} + j' \frac{\mathrm{D} \mathbf{x}}{\mathrm{D} t} - \dot{s} \left(\frac{\mathrm{D} \mathbf{x}}{\mathrm{D} t} \right)_{,s} - \mathbf{g} \right] \cdot \delta \mathbf{x} + \left[\gamma\, \dot{s} \left(\frac{\mathrm{D} \mathbf{x}}{\mathrm{D} t} - \dot{s}\, \mathbf{x}_{,s} \right) + N\, \mathbf{x}_{,s} \right] \cdot \delta \mathbf{x}_{,s} + B\, \mathbf{x}_{,ss} \cdot \delta \mathbf{x}_{,ss} \right\} \mathrm{d} s$$

$$- \sum_{q}^{Q} \mathbf{F}_q(t) \cdot \mathbf{x}(t, s_q^*) + \mathbf{R}_1 \cdot \delta \mathbf{x}(s_1) + M_1\, \mathbf{n}_1 \cdot \delta \mathbf{x}_{,s}(s_1) = 0,$$

$$\left\{ - \left(\frac{\gamma}{2} \dot{\mathbf{x}}^2 - \frac{B}{2} \mathbf{x}_{,ss}^2 + \gamma \mathbf{g} \cdot \mathbf{x} \right) + \mathcal{T}_{C1,s_1} - (\mathcal{T}_{C1,\dot{s}_1})_{,t} - \mathcal{V}_{C1,s_1} + (\mathcal{V}_{C1,\dot{s}_1})_{,t} - \mathbf{R}_1 \cdot \mathbf{x}_{,s}(s_1) - M_1\, \mathbf{n}_1 \cdot \mathbf{x}_{,ss}(s_1) \right\} \delta s_1 = 0. \tag{40}$$

4 Numerical FE scheme for the ALE formulation

A FE model is developed for reconstructing the unknown fields of the position $\mathbf{x}(t, s)$ and of the internal axial force $N(t, s)$ within the time-varying subdomain $\mathcal{N}(t)$ through the use of discrete data. Similarly to classical FE approaches, the reconstructed fields should fulfill the continuity of the physical fields. However, differently from the classical Lagrangian formulations, the quantities are defined on the moving mesh in the ALE approach, meaning that the time derivatives obtained from the reconstruction of the time derivatives of the discrete degrees of freedom are in fact *material* time derivatives.

In order to adopt an adequate reconstruction of the continuous fields $\mathbf{x}(t, s)$ and $N(t, s)$, the function spaces to which these fields belong must first be defined. To capture the nonlinear dynamics of an inextensible flexible rod, as in the cases described in Sections 3.1 and 3.2, $\mathbf{x}(t, s)$ and $N(t, s)$ should be C^1 and C^0 continuous in the time-varying subdomain $\mathcal{N}(t)$. Further, since weak solutions to Eq. (30) are sought, the inner products of $\mathbf{x}(t, s)$,

$\mathbf{x}_{,s}(t,s)$, $\mathbf{x}_{,ss}(t,s)$, and $N(t,s)$ with their variations (belonging to the same function spaces) need to be defined. Therefore, $\mathbf{x}$, N, and their variations should belong to the Hilbert spaces $\mathsf{H}^2(\mathcal{N})$ and $\mathsf{H}^1(\mathcal{N})$ respectively, where the notation $\mathsf{H}^k(\mathcal{N})$ is employed to denote the Sobolev space $\mathsf{W}^{k,2}(\mathcal{N})$ over the real numbers, with $\mathsf{H}^0(\mathcal{N}) \equiv \mathsf{L}^2(\mathcal{N})$, and $\mathsf{L}^2(\mathcal{N})$ is the space of the square-integrable functions in $\mathcal{N}$.

To facilitate the reconstruction using finite elements, subdomain $\mathcal{N}$ is partitioned in N_{el} non-overlapping elements covering the subdomains $\Omega_i = [\hat{s}_i, \hat{s}_{i+1}]$, with $\hat{s}_1 = s_1(t)$ and $\hat{s}_{N_{el}+1} = s_2(t)$. Then, the reconstructed fields (denoted with $(\hat{\cdot})$) can be written as

$$\hat{\mathbf{x}}(t,s) = \mathbf{H}(\hat{\sigma}(s)) \cdot \hat{\mathbf{x}}_i(t), \quad \hat{N}(t,s) = \mathbf{P}(\hat{\sigma}(s)) \cdot \hat{\mathbf{N}}_i(t), \quad s \in \Omega_i, \tag{41}$$

where the linear map $\hat{\sigma}(s;i) : (\hat{s}_i, \hat{s}_{i+1}) \to (0,1)$ is the element-local position parameter, $\mathbf{H}(\hat{\sigma})$, and $\mathbf{P}(\hat{\sigma})$ are the interpolation matrices for the fields $\mathbf{x}$ and N over Ω_i,

$$\mathbf{H}(\hat{\sigma}) = [\, h_1(\hat{\sigma})\,\mathbf{I} \mid h_2(\hat{\sigma})\,\mathbf{I} \mid h_3(\hat{\sigma})\,\mathbf{I} \mid h_4(\hat{\sigma})\,\mathbf{I} \,], \quad \mathbf{P}(\hat{\sigma}) = [\, p_1(\hat{\sigma}) \mid p_2(\hat{\sigma}) \,], \tag{42}$$

with $h_k(\hat{\sigma}), k = 1, \ldots, 4$ being the four two-node Hermite basis functions of $\mathsf{H}^2(\Omega_i)$, $p_k(\hat{\sigma}), k = 1, 2$ the two Lagrange basis functions of $\mathsf{H}^1(\Omega_i)$, and $\mathbf{I}$ is the identity matrix of appropriate size [63]. The vectors $\hat{\mathbf{x}}_i$, and $\hat{\mathbf{N}}_i$ collect the degrees of freedom of the discrete reconstruction associated with the i-th element. Further, if the entirety of the degrees of freedom is collected in the vectors $\hat{\mathbf{x}}(t)$ and $\hat{\mathbf{c}}(t)$, where $\hat{\mathbf{c}}(t) = [\hat{\mathbf{N}}, \mathbf{R}_1, M_1, \mathbf{R}_2, M_2]^T$ collects all the degrees of freedom associated with the constraints, the space-discrete governing equations can be written in matrix form as

$$\begin{bmatrix} \mathbf{M}_{xx} & 0 \\ 0 & 0 \end{bmatrix} \cdot \begin{pmatrix} \ddot{\hat{\mathbf{x}}} \\ \ddot{\hat{\mathbf{c}}} \end{pmatrix} + \begin{bmatrix} \mathbf{C}_{xx} & 0 \\ 0 & 0 \end{bmatrix} \cdot \begin{pmatrix} \dot{\hat{\mathbf{x}}} \\ \dot{\hat{\mathbf{c}}} \end{pmatrix} + \begin{bmatrix} \mathbf{K}_{xx} & \mathbf{K}_{xc}(\hat{\mathbf{x}}) \\ \mathbf{K}_{cx}(\hat{\mathbf{x}}) & 0 \end{bmatrix} \cdot \begin{pmatrix} \hat{\mathbf{x}} \\ \hat{\mathbf{c}} \end{pmatrix} = \begin{pmatrix} \mathbf{F}_x \\ \mathbf{F}_c \end{pmatrix}, \tag{43}$$

where

$$\mathbf{M}_{xx} = \mathcal{A}\left(\int_{\hat{s}_i}^{\hat{s}_{i+1}} \gamma\, \mathbf{H}^T \mathbf{H}\, \mathrm{d}s \right), \; \mathbf{K}_{xx} = \mathcal{A}\left(\int_{\hat{s}_i}^{\hat{s}_{i+1}} \left[B\, \mathbf{H}_{,ss}^T \mathbf{H}_{,ss} - \gamma\, \dot{s}^2\, \mathbf{H}_{,s}^T \mathbf{H}_{,s} - \gamma\, \ddot{s}\, \mathbf{H}^T \mathbf{H}_{,s} \right] \mathrm{d}s \right),$$

$$\mathbf{K}_{xc} = \mathcal{A}\left(\int_{\hat{s}_i}^{\hat{s}_{i+1}} \mathbf{H}_{,s}^T \mathbf{x}_{,s} \mathbf{P}\, \mathrm{d}s \right) + \mathcal{A}_{R1}\left(\mathbf{H}^T(0) \right) + \mathcal{A}_{M1}\left(\mathbf{H}_{,s}^T(0)\mathbf{n}_1 \right) + \mathcal{A}_{R2}\left(\mathbf{H}^T(1) \right) + \mathcal{A}_{M2}\left(\mathbf{H}_{,s}^T(1)\mathbf{n}_2 \right),$$

$$\mathbf{K}_{cx} = \mathcal{A}^T\left(\frac{1}{2} \int_{\hat{s}_i}^{\hat{s}_{i+1}} \mathbf{P}^T \mathbf{x}_{,s} \mathbf{H}_{,s}\, \mathrm{d}s \right) + \mathcal{A}_{R1}^T\left(\mathbf{H}(0) \right) + \mathcal{A}_{M1}^T\left(\mathbf{n}_1^T \mathbf{H}_{,s}(0) \right) + \mathcal{A}_{R2}^T\left(\mathbf{H}(1) \right) + \mathcal{A}_{M2}^T\left(\mathbf{n}_2^T \mathbf{H}_{,s}(1) \right),$$

$$\tag{44}$$

$$\mathbf{C}_{xx} = \mathcal{A}\left(\gamma \int_{\hat{s}_i}^{\hat{s}_{i+1}} \left[j'\, \mathbf{H}^T \mathbf{H} + \dot{s}\, \left(\mathbf{H}_{,s}^T \mathbf{H} - \mathbf{H}^T \mathbf{H}_{,s} \right) \right] \mathrm{d}s \right),$$

$$\mathbf{F}_x = \mathcal{A}\left(\gamma \int_{\hat{s}_i}^{\hat{s}_{i+1}} \mathbf{H}^T \mathbf{g}\, \mathrm{d}s \right) + \sum_i \mathcal{A}_i\left(H^T(\hat{\sigma}(s_i^*))\, \mathbf{F}_{ext} \right),$$

$$\mathbf{F}_c = \mathcal{A}\left(\int_{\hat{s}_i}^{\hat{s}_{i+1}} \mathbf{P}^T\, \mathrm{d}s \right) + \mathcal{A}_{R1}^T\left(\mathbf{a}_1 \right) + \mathcal{A}_{R2}^T\left(\mathbf{a}_2 \right),$$

and $\mathcal{A}$, $\mathcal{A}_{Ri}$, $\mathcal{A}_{Mi}$ are the appropriate assembly operators correlating local matrices to global degrees of freedom, and the superscript T stands for the transpose operator. Finally, this system of equations is augmented by the interface conditions $(30)_2$, in order to balance the number of equations and the unknowns $\hat{\mathbf{x}}$, $\hat{\mathbf{c}}$, and $\mathbf{p}$.

The Newmark method is used for the time integration of the discretized governing equations [63], as it provides a stable, simple, and very efficient way to advance from one timestep to the next. Indeed, if the values $\mathbf{q}^n$ and $\mathbf{q}^{n+1}$ denote the value of the quantity $\mathbf{q}$ associated with times t^n and $t^{n+1} = t^n + \tau$ respectively (being $\tau > 0$ the timestep size), the approximation

$$\mathbf{q}^{n+1} = \mathbf{q}^n + \tau\, \dot{\mathbf{q}}^n + \frac{\tau^2}{2}\left[(1 - 2\beta_1)\, \ddot{\mathbf{q}}^n + 2\beta_1\, \ddot{\mathbf{q}}^{n+1} \right], \qquad \dot{\mathbf{q}}^{n+1} = \dot{\mathbf{q}}^n + \tau\left[(1 - \beta_2)\, \ddot{\mathbf{q}}^n + \beta_2\, \ddot{\mathbf{q}}^{n+1} \right], \tag{45}$$

can be used to solve the nonlinear system (43) for accelerations using an iterative process for each timestep; i.e. Newton-Raphson iterations (under a tolerance 10^{-7}). The coefficients $\beta_1 \in [0, 1/2]$ and $\beta_2 \in [0, 1]$ define the character of the time-integration [63] and are assumed in the following as $\beta_1 = 0.255$ and $\beta_2 = 0.505$. This choice follows from the fact that the usually adopted values $\beta_1 = 0.25$ and $\beta_2 = 0.5$ (middle point rule), providing in classical problems energy conservation, would instead lead to numerical instabilities in the ALE formulation.

In this case the existence of terms with quadratic dependence on the degrees of freedom introduces terms of $O(\tau^4)$ in the system of equations and thus there exists a lower limit for τ when the terms $O(\tau^4)$ become insignificant compared to terms of $O(\tau)$ and constants. Then the limitations of the machine precision may lead to inaccuracies in the solution and subsequently the convergence of the time-stepping algorithm suffers. This can be improved significantly by solving for $\left(\hat{\mathbf{x}}, \hat{\mathbf{N}}\right)^T$ and substituting $\left(\dot{\hat{\mathbf{x}}}, \dot{\hat{\mathbf{N}}}\right)^T$ and $\left(\ddot{\hat{\mathbf{x}}}, \ddot{\hat{\mathbf{N}}}\right)^T$ via Eq. (45). This approach introduces terms of at most $O(\tau^2)$.

Then, the fully discretized nonlinear equations to be solved at every timestep $n+1$ can be written as

$$\mathbf{f}(\hat{\mathbf{x}}^{n+1}, \hat{\mathbf{c}}^{n+1}; \mathbf{p}^{n+1}) = \begin{bmatrix} \frac{1}{\tau^2 \beta_1}\mathbf{M}_{xx}^{n+1} + \frac{\beta_2}{\tau\beta_1}\mathbf{C}_{xx}^{n+1} + \mathbf{K}_{xx}^{n+1} & \mathbf{K}_{xc}^{n+1} \\ \mathbf{K}_{cx}^{n+1} & 0 \end{bmatrix} \begin{pmatrix} \hat{\mathbf{x}}^{n+1} \\ \hat{\mathbf{c}}^{n+1} \end{pmatrix} - \begin{pmatrix} \mathbf{b}_x^{n+1} \\ \mathbf{F}_c^{n+1} \end{pmatrix} = \mathbf{0}, \tag{46}$$

$$\mathbf{g}(\hat{\mathbf{x}}^{n+1}, \hat{\mathbf{c}}^{n+1}; \mathbf{p}^{n+1}) = \mathbf{0},$$

where

$$\mathbf{b}_x^{n+1} = \mathbf{F}_x^{n+1} + \mathbf{M}_{xx}^{n+1} \cdot \left[\frac{1}{\tau^2 \beta_1}\hat{\mathbf{x}}^n + \frac{1}{\tau\beta_1}\dot{\hat{\mathbf{x}}}^n + \frac{1 - 2\beta_1}{2\beta_1}\ddot{\hat{\mathbf{x}}}^n \right] + \mathbf{C}_{xx}^{n+1} \cdot \left[\frac{\beta_2}{\tau\beta_1}\hat{\mathbf{x}}^n - \left(1 - \frac{\beta_2}{\beta_1}\right)\dot{\hat{\mathbf{x}}}^n - \tau\left(1 - \frac{\beta_2}{2\beta_1}\right)\ddot{\hat{\mathbf{x}}}^n \right]. \tag{47}$$

The Jacobian matrix $\mathbf{J}$ has to be considered for implementing the Newton-Raphson method. From Eq. (46) it follows that $\mathbf{J}$ is a block matrix involving large blocks of null elements. More specifically, for the timestep $n + 1$, $\mathbf{J}$ has the following form

$$\mathbf{J} = \begin{bmatrix} \mathbf{J}_{11} & \mathbf{J}_{1p} \\ \mathbf{J}_{p1} & \mathbf{J}_{pp} \end{bmatrix} = \begin{bmatrix} \nabla_{\hat{\mathbf{x}}^{n+1}, \hat{\mathbf{c}}^{n+1}}\mathbf{f} & \nabla_{\hat{\mathbf{p}}^{n+1}}\mathbf{f} \\ \nabla_{\hat{\mathbf{x}}^{n+1}, \hat{\mathbf{c}}^{n+1}}\mathbf{g} & \nabla_{\hat{\mathbf{p}}^{n+1}}\mathbf{g} \end{bmatrix} \tag{48}$$

and the matrix $\mathbf{J}_{11}$ can be evaluated easily in the absence of solution dependent forces (i.e. nonlinear viscous damping, friction). Further, being a block matrix, the form of $\mathbf{J}$ can be used to write the inverse $\mathbf{J}^{-1}$ as a function of inverses of matrices of smaller dimensions as follows

$$\mathbf{J}^{-1} = \begin{bmatrix} \mathbf{J}_{11}^{-1} + \mathbf{J}_{11}^{-1} \cdot \mathbf{J}_{1p} \cdot \bar{\mathbf{J}}^{-1} \cdot \mathbf{J}_{p1} \cdot \mathbf{J}_{11}^{-1} & -\mathbf{J}_{11}^{-1} \cdot \mathbf{J}_{1p} \cdot \bar{\mathbf{J}}^{-1} \\ -\bar{\mathbf{J}}^{-1} \cdot \mathbf{J}_{p1} \cdot \mathbf{J}_{11}^{-1} & \bar{\mathbf{J}}^{-1} \end{bmatrix}, \tag{49}$$

where $\bar{\mathbf{J}}$ is the Schur complement of matrix $\mathbf{J}$ with respect to block $\mathbf{J}_{11}$,

$$\bar{\mathbf{J}} = \mathbf{J}_{pp} - \mathbf{J}_{p1} \cdot \mathbf{J}_{11}^{-1} \cdot \mathbf{J}_{1p}. \tag{50}$$

In turn, $\mathbf{J}_{11}^{-1}$ can be calculated using the same technique as

$$\mathbf{J}_{11}^{-1} = \begin{bmatrix} \mathbf{J}_{xx}^{-1} + \mathbf{J}_{xx}^{-1} \cdot \mathbf{J}_{xc} \cdot \bar{\mathbf{J}}_{11}^{-1} \cdot \mathbf{J}_{cx} \cdot \mathbf{J}_{xx}^{-1} & -\mathbf{J}_{xx}^{-1} \cdot \mathbf{J}_{xn} \cdot \bar{\mathbf{J}}_{11}^{-1} \\ -\bar{\mathbf{J}}_{11}^{-1} \cdot \mathbf{J}_{cx} \cdot \mathbf{J}_{xx}^{-1} & \bar{\mathbf{J}}_{11}^{-1} \end{bmatrix}, \tag{51}$$

where $\bar{\mathbf{J}}_{11}$ is the Schur complement of matrix $\mathbf{J}_{xx}$

$$\bar{\mathbf{J}}_{11} = -\mathbf{J}_{cx} \cdot \mathbf{J}_{xx}^{-1} \cdot \mathbf{J}_{xc}. \tag{52}$$

The discretized equations are solved numerically using in-house software developed in Matlab, the source code of which is publicly available [62].

Table 1: Numerical data and expressions used for the three case studies (CS-1, CS-2, and CS-3) and the two instability problems (IP-1 and IP-2).

Data	Units	CS-1	CS-2	CS-3	IP-1	IP-2		
L	[m]	1	2	3	2	5		
B	[Nm^2]	2	2.8	0.15	1	1		
γ	[kg/m]	0	0.312	0.4	10^{-5}	0.05		
m	[kg]	1	-	-	0.999 m_{tr} 1.001 m_{tr}	-		
ℓ_0	[m]	0.4694	1	1	1	1		
θ_1	[rad]	$\frac{2\pi}{3}$	$\frac{\pi}{2}$	0	$\frac{\pi}{4}$	ωt		
θ_2	[rad]	-	-	0	-	$\pm\omega t$		
ω	[rad/s]	-	-	-	-	0.5 $\mid$ 0.2 $\mid$ 0.02 $\mid$ 10^{-3}		
Gravity acc.	-	yes	yes	yes	yes	no		
Force	[N]	-	$\sin(4\pi t)$	-	-	-		
Dissipation	-	-	-	$c=\{0,1\}$Ns/m	$\zeta=0.025, \mu = 0.15$	-		
τ	[s]	10^{-4}	10^{-4}	10^{-3}	10^{-5}	$2 \cdot 10^{-3}$ $\mid$ 0.1		

5   Validation by case studies and application to instability problems

Three case studies (CS-1, CS-2, and CS-3) and two instability problems (IP-1 and IP-2) are addressed to assess the capability and reliability of the presented ALE formulation. The time-varying subdomain $\mathcal{N}(t)$ of these five mechanical systems is discretized through the same number of elements, $N_{el} = 32$, while the other numerical data are summarized in Table 1. The convergence of the results with mesh refinement is also investigated by varying N_{el} for two case studies (CS-2 and CS-3).

5.1   Case studies

CS-1:   A massless elastic rod has a lumped mass m attached at one end $(s = L)$ and is constrained at the other end by a sliding sleeve with constant inclination $\theta_1 = 2\pi/3$. A gravity acceleration field is present, opposite to the x_2 axis and of magnitude $g = 9.81$m/s^2. The system evolution is analyzed for the 3s just after the release time $t = 0$ from initial rest conditions, where the rod has an initial external length $\ell_0 = L - s_1(0)$. The results from the numerical integration are reported as the trajectory of the lumped mass in Fig. 3(left) with a blue line marked with circles and as the evolution of the configuration parameter $s_1(t)$ in Fig. 3(right). Results from the same system obtained from a different ALE formulation proposed by Han [57] are also reported in Fig. 3 with a dashed black line, showing excellent accordance between the two ALE formulations.

CS-2:   Mass convection effects are activated by considering a rod with a non-null linear mass density γ. The rod is constrained by one sliding sleeve with constant inclination $\theta_1 = \pi/2$ and loaded, in addition to a gravity field as for CS-1, through a time-harmonic force $F(t) = \sin(4\pi t)$ acting at the curvilinear coordinate $s = L$ with constant direction, parallel to the x_1 axis. Assuming initial rest conditions and an initial external length $\ell_0 = 1$m, the evolution until final ejection of the rod (occurring at $t = t_{eje} \approx 0.563$s) obtained from the present method is reported in Fig. 4 for the displacement components $u_1(t) = x_1(t, L) - x_1(0, L)$ (solid red) and $u_2(t) = x_2(t, L) - x_2(0, L)$ (solid yellow) at the edge $s = L$ and for the configuration parameter $s_1(t)$ (solid blue). These results are validated through comparison with the numerical results available in [58], also included in Fig. 4 with dashed black lines. It is noted that the system becomes unconstrained for $t > t_{eje}$ and therefore its dynamics can be solved by standard methods afterwards.

The kinetic $\mathcal{T}$ and potential $\mathcal{V}$ energies, the negative of the external work $\mathcal{W}$ of the time-harmonic force, and the
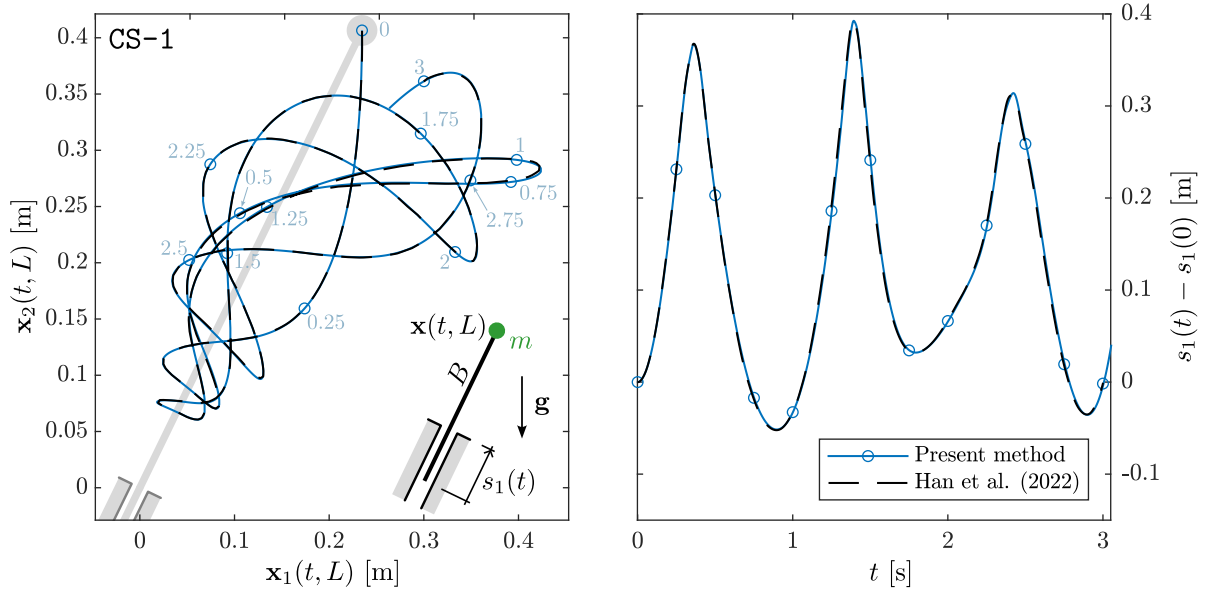
Figure 3: (Left) Trajectory of the lumped mass m attached at the curvilinear coordinate $s = L$ and (Right) evolution in time of the insertion length difference $s_1(t) - s_1(0)$ for CS-1. Results obtained with the present method (solid blue line) are superimposed to those by Han [57] (dashed black line). Specific position at time $t = (0.25j)$s $(j = 1, ..., 12)$ is highlighted along the trajectory.
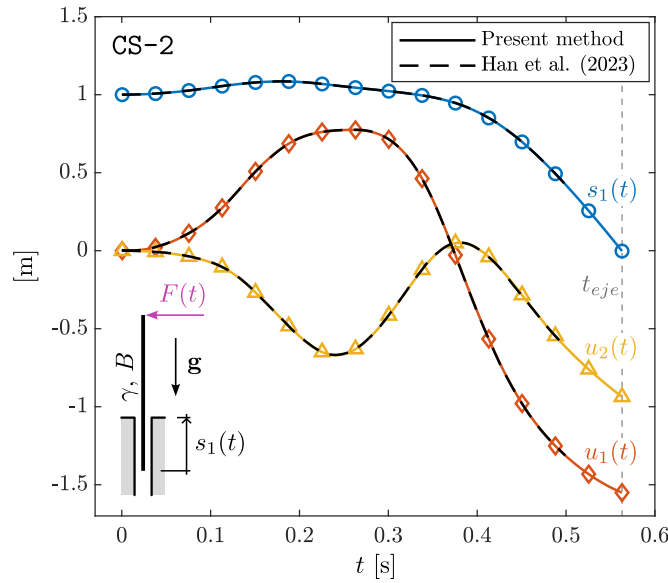

Figure 4: Evolution in time t of the displacement components $u_1(t)$ (red) and $u_2(t)$ (yellow) of the unconstrained rod's end $(s = L)$ and of the insertion length $s_1(t)$ (blue) for CS-2. The system evolution ends with a final ejection of the rod at $t = t_{eje} \approx 0.563$s. Results obtained from the present method (continuous lines) are perfectly superimposed to those by Han and Bachau [58] (dashed lines).

15

total energy $\mathcal{E} = \mathcal{T} + \mathcal{V} - \mathcal{W}$ of the whole system is reported in Fig. 5(left) as a function of time. It is observed that, although the energy appears conserved, advection effects inherent to the ALE formulation introduce a deviation in time of the total energy $\mathcal{E}(t)$ from its initial value $\mathcal{E}(0)$ during fast dynamics transients, as shown in the inset (drawn by magnifying the vertical axis). To overcome such a small violation of energy conservation, an upwind biased numerical scheme can potentially be used. The results for the energies (Fig. 5, left) are complemented by the time derivative of the total energies $\mathcal{E}_{\mathcal{N}} = \mathcal{T}_{\mathcal{N}} + \mathcal{V}_{\mathcal{N}} - \mathcal{W}$ (blue) and $\mathcal{E}_{\mathcal{C}_1} = \mathcal{T}_{\mathcal{C}_1} + \mathcal{V}_{\mathcal{C}_1}$ (red), respectively associated to the two subdomains $\mathcal{N}(t)$ and $\mathcal{C}_1(t)$ in Fig. 5(right). In addition to these two curves, a third curve in black representing $d\mathcal{E}/dt = d(\mathcal{E}_{\mathcal{N}} + \mathcal{E}_{\mathcal{C}_1})/dt$ is reported, confirming that, no significant energy change occurs for the whole system, although each rod's subportion displays a varying energy in time.

Finally, it is noted that the reported curves are obtained by assuming a unit value for the initial total energy, $\mathcal{E}(0) = 1\text{Nm}$.
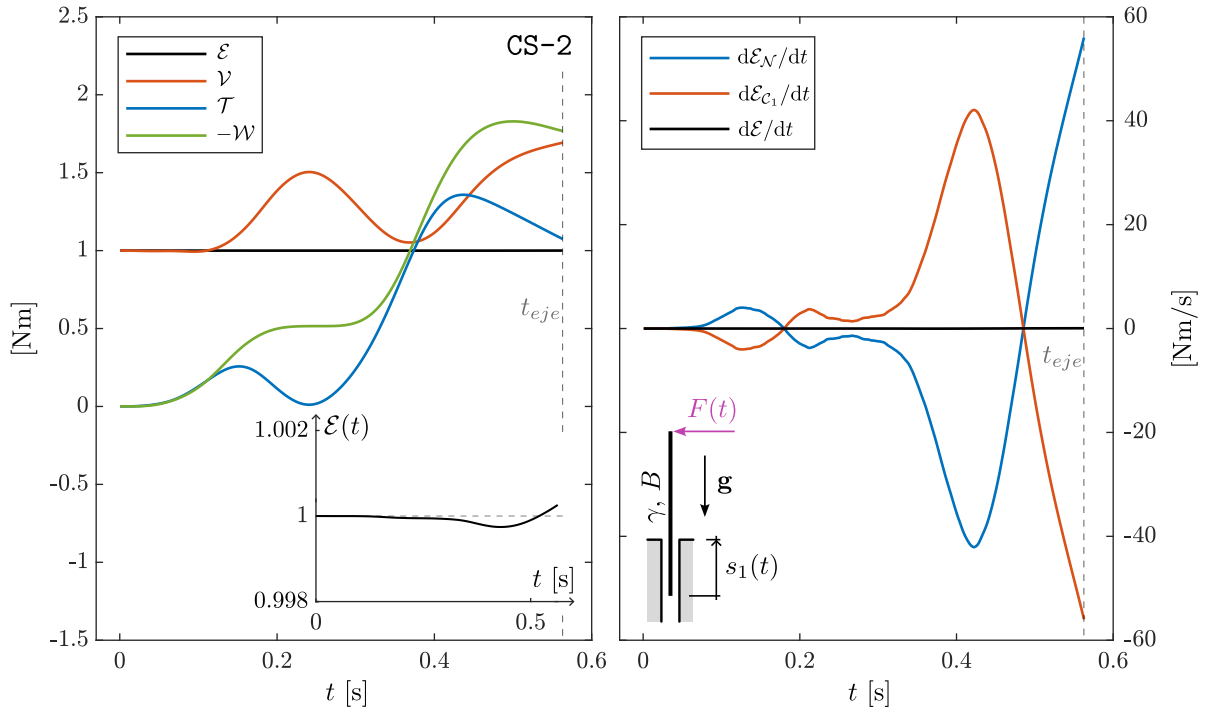

Figure 5: (Left) Total $\mathcal{E}$ (black), potential $\mathcal{V}$ (red), and kinetic $\mathcal{T}$ (blue) energies, and the negative of the work of the external force $\mathcal{W}$ (green) as a function of time t for CS-2, until $t = t_{eje} \approx 0.563$s when the final ejection of the rod occurs. A magnification of the total energy $\mathcal{E}$ curve is also included in the inset to highlight the violation of the conservation of energy principle by the numerical integration scheme. (Right) Time derivative of the total energies $\mathcal{E}_{\mathcal{N}}$ (blue) and $\mathcal{E}_{\mathcal{C}_1}$ (red) respectively associated with the varying subdomains $\mathcal{N}(t)$ and $\mathcal{C}_1(t)$. The time derivative of these two quantities are of equal measure and opposite as shown by the black line representing the derivative in time of the total energy $\mathcal{E}$ of the whole system.

CS-3: A rod with non-null mass density γ within a gravity field, defined as in CS-1, is constrained by two sliding sleeves aligned along the x_1 axis and at a distance $(\mathbf{a}_2 - \mathbf{a}_1) \cdot \mathbf{e}_1 = 1$m from each other, where $\mathbf{e}_1$ is the unit vector parallel to the x_1 axis. Dissipation is introduced as a distributed transverse loading along the subdomain $\mathcal{N}(t)$ as

$$\mathbf{F}_{dissip} = -c\,\mathbf{v}_{\perp}(t) \tag{53}$$

16

where $\mathbf{v}_\perp = \dot{\mathbf{x}} - \mathbf{x}_{,s}(\mathbf{x}_{,s} \cdot \dot{\mathbf{x}})$ is the component of the velocity $\dot{\mathbf{x}}$ perpendicular to the rod and $c \geq 0$ is the dissipation coefficient. From an initial rest condition, the system evolves with oscillations of decaying amplitude whenever $c > 0$. The evolution is displayed through the values of $s_1(t) - s_1(0)$ (blue), $u_1(t) = x_1(t, L/2) - x_1(0, L/2)$ (red), $u_2(t) = x_2(t, L/2) - x_2(0, L/2)$ (yellow) in Fig. 6 for the first 10 s just after the release time for the conservative system ($c = 0$, top left) and the non-conservative one ($c = 1\text{Ns/m}$, top right). The deformed configuration at $t = 7.772$s is shown in Fig. 6(bottom) for the subdomain $\mathcal{N}$ of these two systems ($c = 0$ blue, $c = 1\text{Ns/m}$ green) along with part of the fully constrained portions $\mathcal{C}_1$ and $\mathcal{C}_2$. The time $t = 7.772$s is selected as providing the (periodic) maximum deflection of the rod for the conservative system ($c = 0$).
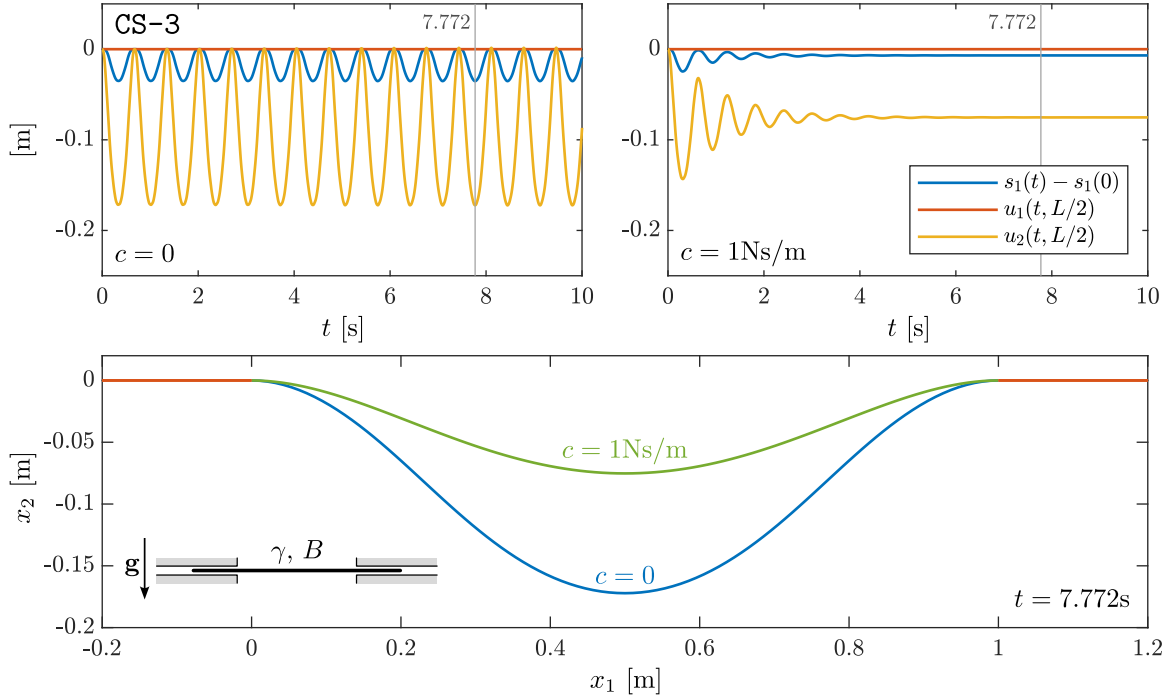
Figure 6: (Top) Evolution in time t of $s_1(t) - s_1(0)$ (blue) and of the displacement components $u_1(t) = x_1(t, L/2) - x_1(0, L/2)$ (red), $u_2(t) = x_2(t, L/2) - x_2(0, L/2)$ (yellow) associated to the rod's mid point ($s = L/2$) for CS-3. Two cases are considered, one with null dissipation ($c = 0$, top left) and the other with a non-null dissipation ($c = 1\text{Ns/m}$, top right). (Bottom) Deformed shape of the rod at time $t = 7.772$s for the undissipated ($c = 0$, blue curve) and dissipated ($c = 1\text{Ns/m}$, green curve) systems.

5.2 Convergence of mesh, timestep size and inextensibility constraint

Case studies CS-2 and the undissipated version of CS-3 are further investigated to analyze the solution convergence by varying the number of elements through the sequence $N_{el} = 2^n, n = 1, .., 6$, under a constant timestep $\tau = 5 \cdot 10^{-4}$s. The L^2 error estimates for the trajectory of the deformed shape and the configuration parameter vector $\mathbf{p}$, with respect to corresponding values for the case with $N_{el} = 128$ (considered here as the target solution) are evaluated as

$$\epsilon_{\mathbf{x}} = \left[\int_0^1 [\mathbf{x}_{N_{el}}(t_c, s(t_c, \sigma)) - \mathbf{x}_{128}(t_c, s(t_c, \sigma))]^2 \, \mathrm{d}\sigma \right]^{\frac{1}{2}}, \qquad \epsilon_{\mathbf{p}} = ||\mathbf{p}_{N_{el}}(t_c) - \mathbf{p}_{128}(t_c)||, \tag{54}$$

and, similarly, for the time derivatives the error estimates as

$$\epsilon_{\dot{\mathbf{x}}} = \left[\int_0^1 \left[\dot{\mathbf{x}}_{N_{el}}(t_c, s(t_c, \sigma)) - \dot{\mathbf{x}}_{128}(t_c, s(t_c, \sigma)) \right]^2 d\sigma \right]^{\frac{1}{2}}, \qquad \epsilon_{\dot{\mathbf{p}}} = ||\dot{\mathbf{p}}_{N_{el}}(t_c) - \dot{\mathbf{p}}_{128}(t_c)||, \tag{55}$$

where t_c is the reference time at which the convergence is assessed.

The convergence of the error estimates is shown in Fig. 7 for CS-2 (left) and for CS-3 (right). Two reference times are considered for each case study, $t_c = \{0.25, 0.5\}$s for CS-2 and $t_c = \{0.45, 0.9\}$s for CS-3, distinguished by using two different colors. Error estimates are reported for $\epsilon_{\mathbf{x}}$ and $\epsilon_{\mathbf{p}}$ (top) and for $\epsilon_{\dot{\mathbf{x}}}$ and $\epsilon_{\dot{\mathbf{p}}}$ (bottom), evaluated through Eqns (54) and (55). The error estimates related to the trajectory $\mathbf{x}$ (configuration parameter vector $\mathbf{p}$) and to its time derivative are denoted with circle (diamond) markers. The Figure shows that the errors of the solution obtained by the present method decrease exponentially with the number of elements, thus achieving convergence.

5.3 Application to instability problems and prediction of critical conditions

The present method is finally tested through its application to two different instability problems IP-1 and IP-2 for assessing if the evaluated critical values of the input parameters match the respective predictions provided in [56] and in [64]. These examples are important, as they are representative of cases where the loss of stability of an equilibrium configuration leads to fast dynamics. Numerical data considered for IP-1 and IP-2 are summarized in Table 1.

IP-1: This problem is very similar to CS-1 with exception for the values of the input data L, B, θ_1, and the presence of a small self-weight γ in order to include dissipation in the system at two end points of the domain $\mathcal{N}(t)$ within the present formulation. More specifically, dissipation is included through:

- a concentrated viscous force $\mathbf{F}_{visc}(t)$ applied at the lumped mass curvilinear coordinate $s = L$

$$\mathbf{F}_{visc}(t) = -2\zeta \sqrt{\frac{3mB}{(L - s_1(t))^3}} \dot{\mathbf{x}}(t, L), \tag{56}$$

where $\zeta \geq 0$ is the dimensionless viscous dissipation parameter;

- a concentrated Coulomb friction force $\mathbf{F}_{fr}(t)$ at the sliding sleeve exit $(s = s_1(t))$, acting parallel to the sliding direction $\mathbf{b}_1$ and oppositely to the sliding velocity $\dot{s}_1(t)$, defined as

$$\mathbf{F}_{fr}(t) = -\mu \, |\mathbf{R}(t) \cdot \mathbf{n}| \, \text{sgn}(\dot{s}_1(t)) \, \mathbf{b}_1, \tag{57}$$

$$\mathbf{F}_{fr}(t) = -\mu \, \sqrt{(\mathbf{R}(t) \cdot \mathbf{n})^2} \, \frac{\dot{s}_1(t)}{\sqrt{\dot{s}_1^2(t) + \varepsilon}} \, \mathbf{b}_1, \tag{58}$$

where ε is a small quantity, selected as $\varepsilon = 2 \cdot 10^{-6}\text{m}^2/\text{s}^2$.

According to [56], as the result of the dynamic evolution after the release of the undeformed rod from a state of rest, two different final states are expected: either the rod is completely injected inside the sleeve or it is completely ejected from the sleeve. For given values of the bending stiffness B, dissipation parameters (ζ, μ), and of the initial external length ℓ_0, each one of the two different final states is associated to a connected region within the m–θ_1 plane, and the transition between these two behaviours is provided by the monotonic curve $m_{tr}(\theta_1)$. For the angle θ_1 under consideration, the transition value for the lumped mass is found in [56] under the assumption of null linear mass density $(\gamma = 0)$ to be given by $m_{tr}(\theta_1 = \pi/4) \approx 0.184098\text{kg}$.

The results of the present ALE method are shown in Fig. 8 for two different lumped mass values $m = \{0.999, 1.001\} m_{tr}$ attached to a rod with a linear mass density $\gamma = 1.0864 \cdot 10^{-4}\text{kg/m}$ and are compared with the semi-analytical solution based on the Euler's elastica [56] (obtained by assuming $\gamma = 0$). More specifically, the trajectories of the lumped mass m and the time evolution of the length of the rod outside the sleeve $L - s_1(t)$
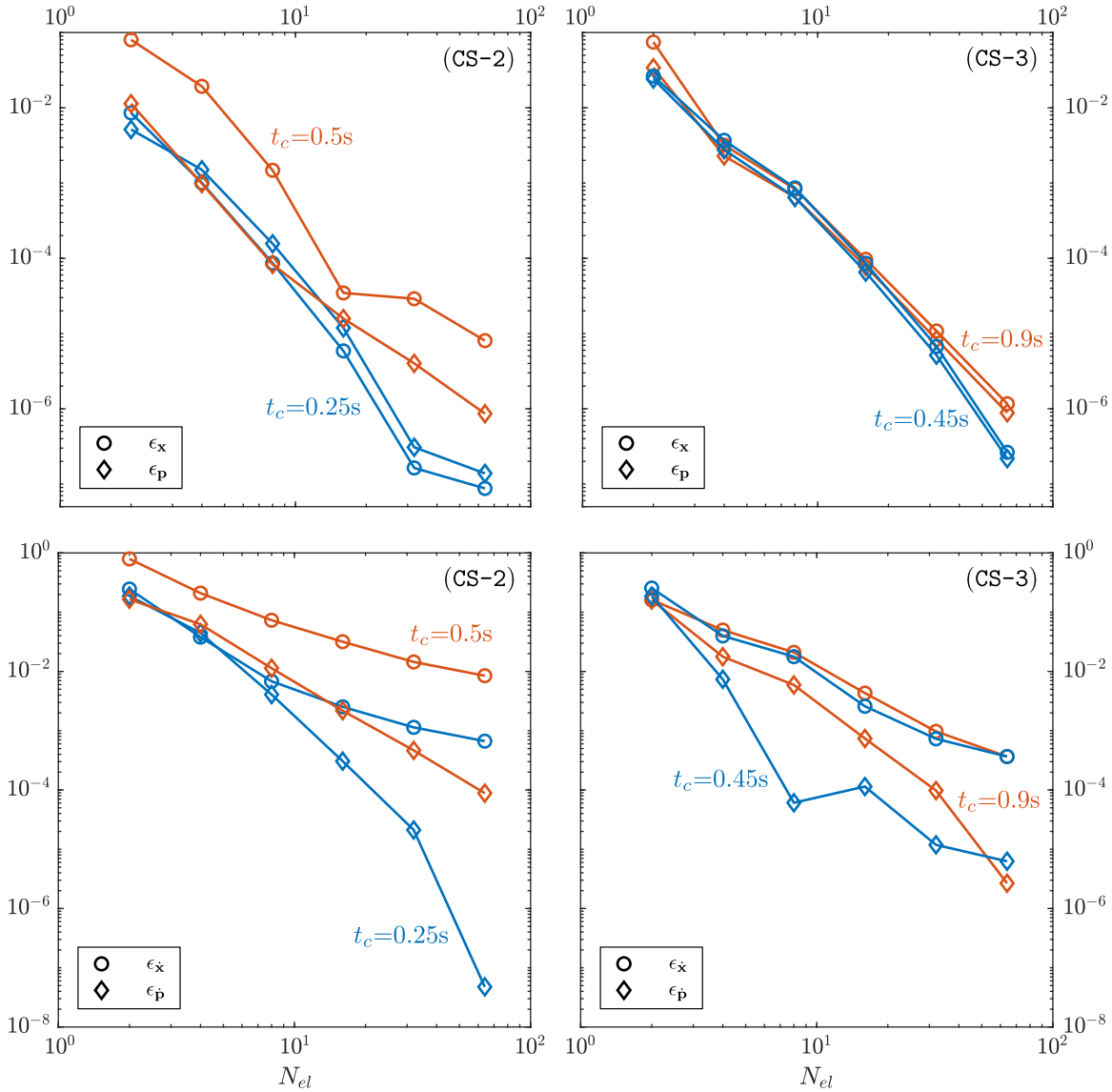
Figure 7: (Left) Convergence analysis for `CS-2` at the two reference times $t_c = 0.25$s (blue lines) and $t_c = 0.5$s (red lines). The top part shows the error estimates for the trajectory $\mathbf{x}$ (circles) and the configuration parameter vector $\mathbf{p}$ (diamonds) at increasing number of elements N_{el} under a timestep $\tau = 5 \cdot 10^{-4}$s, while the lower part shows the error etsimates for their derivatives. (Right) As for left, but for the undissipated version of `CS-3` at $t_c = 0.45$s (blue lines) and $t_c = 0.9$s (red lines).

are reported on the left and on the right of Fig. 8 respectively. The curves corresponding to $m = 0.999\,m_{tr}$ are reported with solid blue lines and to $m = 1.001\,m_{tr}$ with solid red lines, and the results from the present ALE method are reported as continuous while those from [56] as dashed lines.

The discrepancy in the lumped mass trajectory $\mathbf{x}(L, t)$ and in the external rod's length, $L - s_1(t)$, which can be observed for the case $m = 1.001\,m_{tr}$, is inherent to the effect of the distributed mass γ in the vicinity from above of the mass value m to m_{tr}, which is very small ($\gamma = 2.17 \cdot 10^{-4}\,m_{tr}/L$) in the present ALE-FE model, but

null in the elastica-based model by Armanini et al. [56]. Indeed, by definition of critical condition, the response of the rod becomes very sensitive near the transition value m_{tr} and as a consequence even a small difference in the model (such as considering a small, but non-null, distributed inertia) realizes noticeable differences in the results. However, despite this difference in the trajectory, the final state of the system is correctly predicted in both cases.
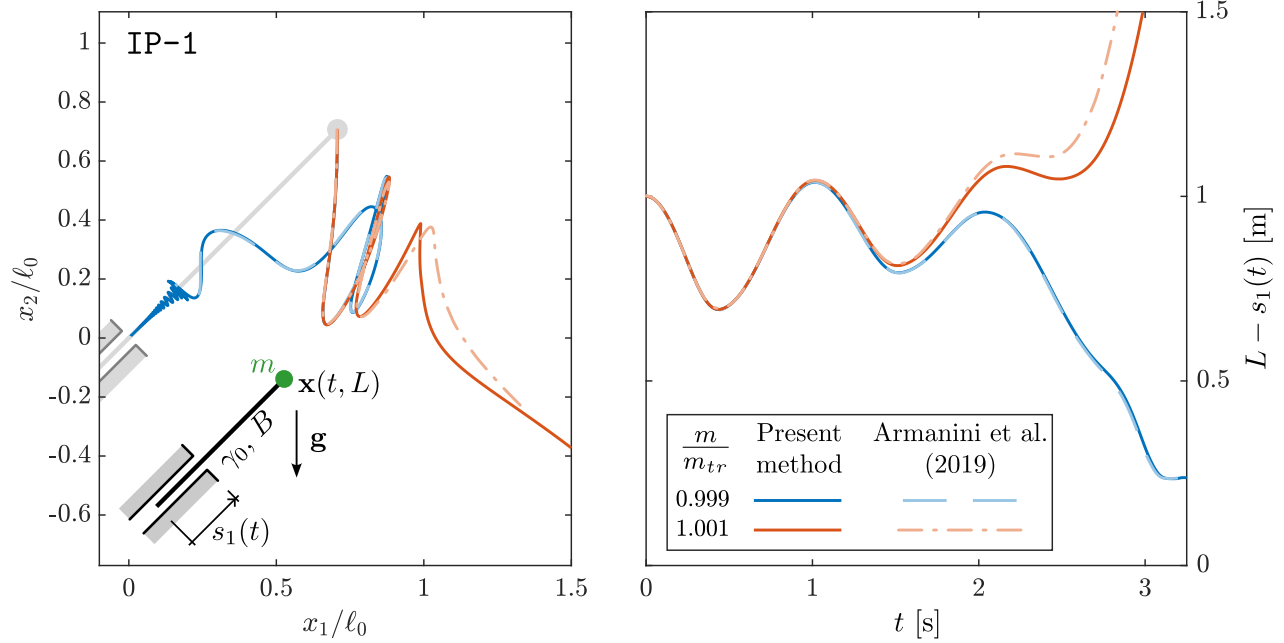

Figure 8: (Left) Trajectory of the lumped mass m attached at the rod's end $s = L$. (Right) Evolution in time of the external rod's length, $L - s_1(t)$. The curves are reported for $m = 0.999 m_{tr}$ (blue) and for $m = 1.001 m_{tr}$ (red), where continuous lines represent the result from the present ALE method while the dashed lines from [56]. The difference in the response between the two models for the value $m = 1.001 m_{tr}$ is due to the high sensitivity of the system near-instability conditions and arises because of the presence of a small distributed inertia γ in the present method, which was considered null in [56].

IP-2: This problem is inspired by the elastica sling system recently presented in [64], where an elastic rod is constrained by two sliding sleeves whose position and inclination can be independently controlled in time. Within a quasi-static setting, critical conditions for the inclination of the sliding sleeve have been found, for which an indefinite ejection of the rod from the constraint is realized, due to the loss of equilibrium stability. This mechanical system is treated here within a dynamic framework by taking into account a non-null linear mass density γ. Without loss of generality, the sliding-sleeves are rotated around their exit points at a constant rate $\theta_1 = \omega t$ and $\theta_2 = \pm \omega t$, where the $+ (-)$ sign realizes a skewsymmetric (symmetric) loading condition. The critical condition within a quasi-static setting is found in [64] to be associated to $\theta_1 = \theta_{cr}$ with $\theta_{cr} \approx 1.7378$rad when $\theta_1 = \theta_2$ and $\theta_{cr} = \pi/2$ when $\theta_1 = \theta_2$. Results from the analysis performed with the present method at different values of the angular velocity $\omega = \{10^{-3}, 0.02, 0.2, 0.5\}$rad/s are reported through the external rod's length $\ell(t) = s_2(t) - s_1(t)$ versus the input rotation $\theta_1(t)$ in Fig. 9 with purple, yellow, red, and blue lines, respectively.

Results for the skewsymmetric loading condition are shown in Fig. 9(left) and for the symmetric one in Fig. 9(right). The critical angle θ_{cr} obtained semi-analytically within a quasi-static setting in [64] is also included as a reference as a vertical dashed black line. In line with previous observations on snapping mechanisms [65, 66, 67], according to which *the higher the angular velocity, the greater the delay*, the present results confirm the delay of the instability due to inertial effect for the elastica sling problem under both loading conditions. On the other hand,

the critical condition evaluated within the quasi-static setting in [64] is recovered for very small angular velocity, $\omega = 10^{-3}$rad/s.
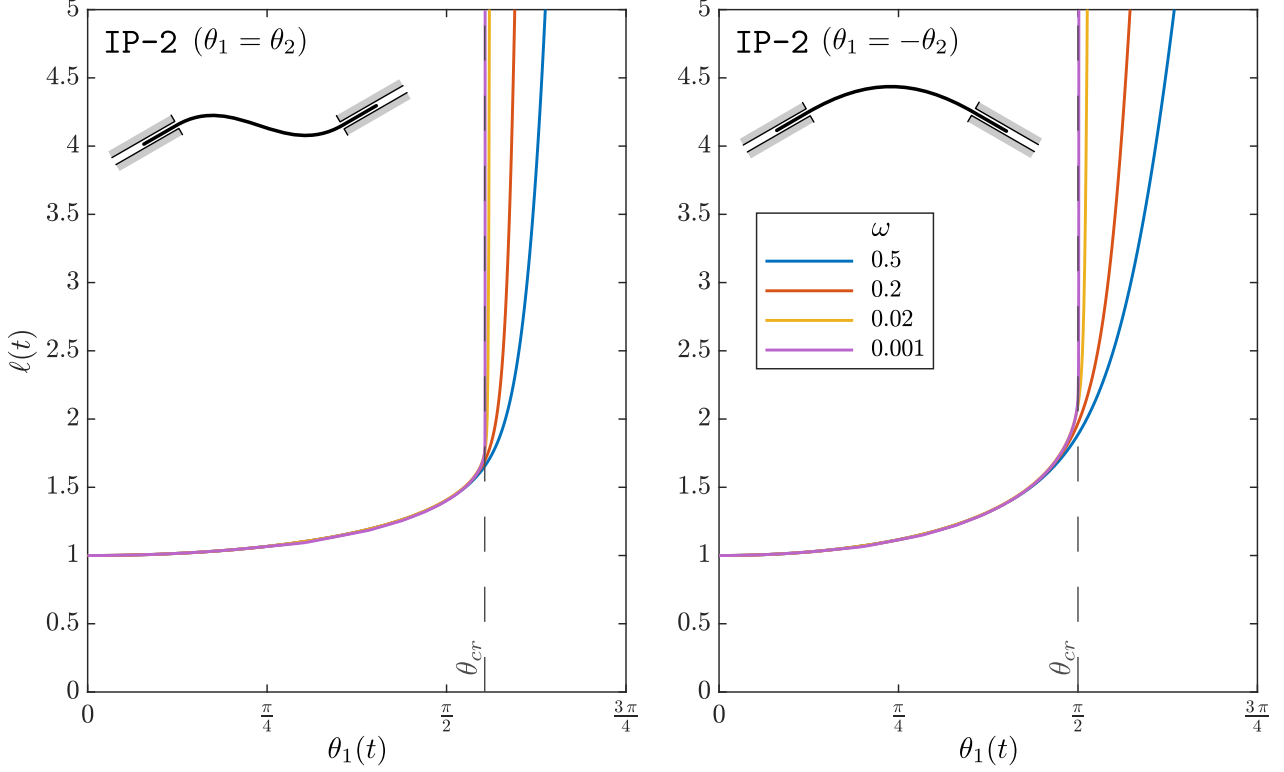

Figure 9: External length $\ell(t) = s_2(t) - s_1(t)$ during the monothonic increase of $\theta_1(t)$ at a constant rate $\omega = \{0.001, 0.02, 0.2, 0.5\}$rad/s, shown with purple, yellow, red, and blue curves respectively. Two loading conditions are reported, skewsymmetric ($\theta_1 = \theta_2$, left) and symmetric ($\theta_1 = -\theta_2$, right). The critical angle θ_{cr} for the uncontrolled ejection evaluated semi-analytically under quasi-static conditions in [64] is shown with a vertical black line, corresponding to $\theta_{cr} = 1.7378$ (left) and to $\theta_{cr} = \pi/2$ (right).

6 Conclusion

An ALE-FE model has been developed for solving the planar nonlinear dynamics of an elastic rod constrained at both ends by sliding sleeves. For this purpose, the mathematical formulation of the mechanics of time variable domains is presented and the first variation of functionals on time-variable domains is derived. Using a position-based description of the rod, the governing equations of the sliding sleeve-rod system are obtained in both the weak and the strong form. The model is based on the idea of a moving mesh defined by an underlying time-variable map, from material coordinates to non-material coordinates. The ALE-FE model is derived by means of a spatial discretization of the relevant fields and the use of the Newmark method for the integration in time. Finally, the numerical model is used to solve some reference case studies and to accurately predict the critical conditions in instability problems, where critical conditions and fast dynamics govern the performance of proposed solutions.

Although a quantitative comparison would require a fair implementation and execution of the methods to be compared, from a qualitative perspective the developed model appears to have the advantage of being faster and easier to implement than the methods currently available. A minor weakness is that, by using the proposed Newmark integration in time, the system energy is only approximately conserved during fast dynamic transients,

due to the advection effects. However, it is expected that this problem could be overcome by the implementation of an upwind biased integration scheme, which is left for future research.

The proposed ALE-FE model, whose source code is made available, provides a powerful yet simple tool to analyze variable-domain mechanical systems and, in turn, to design novel mechanisms for soft actuation, energy harvesting and wave mitigation. It also represents a first step towards an extension for easily developing novel solvers for the three-dimensional dynamics of flexible one- and two-dimensional systems with varying domains.

CRediT authorship contribution statement. P. Koutsogiannakis: Conceptualization; Methodology; Software; Visualization; Validation; Formal analysis; Investigation; Data Curation; Writing - Original Draft; Writing - Review and Editing. T. Papathanasiou: Methodology; Formal analysis; Supervision; Writing - Original Draft; Writing - Review and Editing. F. Dal Corso: Conceptualization; Methodology; Formal analysis; Resources; Supervision; Project administration; Writing - Original Draft; Writing - Review and Editing; Funding acquisition.

References

[1] K. Liu et al. "Triclinic metamaterials by tristable origami with reprogrammable frustration". In: *Advanced Materials* 34.43 (2022), p. 2107998.

[2] S. Zang et al. "Kresling origami mechanics explained: Experiments and theory". In: *Journal of the Mechanics and Physics of Solids* (2024), p. 105630.

[3] L. Zhang et al. "Bistable reconfigurable origami metamaterials with high load-bearing and low state-switching forces". In: *Extreme Mechanics Letters* 63 (2023), p. 102064.

[4] Y. Chen et al. "A programmable auxetic metamaterial with tunable crystal symmetry". In: *International Journal of Mechanical Sciences* 249 (2023), p. 108249.

[5] T. Gao et al. "Shape Programming: Shape Programming by Modulating Actuation over Hierarchical Length Scales (Adv. Mater. 47/2020)". In: *Advanced Materials* 47.32 (2020), n–a.

[6] Y. Peng et al. "Programming bistability in geometrically perturbed mechanical metamaterials". In: *arXiv preprint arXiv:2401.07881* (2024).

[7] H.M.Y.C. Mallikarachchi and S. Pellegrino. "Design of ultrathin composite self-deployable booms". In: *Journal of Spacecraft and Rockets* 51.6 (2014), pp. 1811–1821.

[8] K. Miura and S. Pellegrino. *Forms and Concepts for Lightweight Structures*. Cambridge University Press, 2020.

[9] S. Pellegrino. "Deployable structures". In: Springer, 2001. Chap. Deployable structures in engineering.

[10] J.D. Eshelby. "The Continuum Theory of Lattice Defects". In: *Progress in Solid State Physics*. Ed. by F Seitz and D Turnbull. Vol. 3. Academic Press, 1956, pp. 79–144.

[11] J.D. Eshelby. "The force on an elastic singularity". In: *Philosophical Transactions of the Royal Society of London. Series A, Mathematical and Physical Sciences* 244.877 (1951), pp. 87–112.

[12] D. Bigoni et al. "Eshelby-like forces acting on elastic structures: theoretical and experimental proof". In: *Mechanics of Materials* 80 (2015), pp. 368–374.

[13] M.A. Bukhari and O.R. Barry. "Towards a self tuning sliding mass metastructure". In: *Scientific reports* 11.1 (2021), p. 21630.

[14] L.M. Miller et al. "Experimental passive self-tuning behavior of a beam resonator with sliding proof mass". In: *Journal of Sound and Vibration* 332.26 (2013), pp. 7142–7152.

[15] L.G.H. Staaf et al. "Achieving increased bandwidth for 4 degree of freedom self-tuning energy harvester". In: *Journal of Sound and Vibration* 420 (2018), pp. 165–173.

[16] N. Wicks, B.L. Wardle, and D. Pafitis. "Horizontal cylinder-in-cylinder buckling under compression and torsion: Review and application to composite drill pipe". In: *International Journal of Mechanical Sciences* 50.3 (2008), pp. 538–549.

[17] J.T. Miller et al. "Buckling-induced lock-up of a slender rod injected into a horizontal cylinder". In: *International Journal of Solids and Structures* 72 (2015), pp. 153–164.

[18] L. Demeio and S. Lancioni G. Lenci. "Nonlinear resonances in infinitely long 1D continua on a tensionless substrate". In: *Nonlinear Dynamics* 66 (2011), pp. 271–284.

[19] N.N. Goldberg and O.M. O'Reilly. "Pervasive nonlinear vibrations due to rod-obstacle contact". In: *Nonlinear Dynamics* 103 (2021), pp. 2169–2181.

[20] H. Alfalahi, F. Renda, and C. Stefanini. "Concentric tube robots for minimally invasive surgery: Current applications and future opportunities". In: *IEEE Transactions on Medical Robotics and Bionics* 2.3 (2020), pp. 410–424.

[21] A.Y. Alkayas et al. "Shape and Tip Force Estimation of Concentric Tube Robots Based on Actuation Readings Alone". In: *2023 IEEE International Conference on Soft Robotics (RoboSoft)*. IEEE. 2023, pp. 1–8.

[22] F. Renda et al. "A sliding-rod variable-strain model for concentric tube robots". In: *IEEE Robotics and Automation Letters* 6.2 (2021), pp. 3451–3458.

[23] F. Dal Corso et al. "Nested Bloch waves in elastic structures with configurational forces". In: *Philosophical Transactions of the Royal Society A* 377.2156 (2019), p. 20190101.

[24] M.K. Jaweda et al. "Coiling of elastic rods on rigid substrates". In: *Proceedings of the National Academy of Sciences of the United States of America* 111 (41) (2014), pp. 14663–14668.

[25] J.T. Miller et al. "Buckling of a thin elastic rod inside a horizontal cylindrical constraint". In: *Extreme Mechanics Letters* 3 (2015), pp. 36–44.

[26] Ch. Duriez et al. "New approaches to catheter navigation for interventional radiology simulation". In: *Computer aided surgery* 11.6 (2006), pp. 300–308.

[27] Sh. Li et al. "A novel FEM-based numerical solver for interactive catheter simulation in virtual catheterization". In: *Journal of Biomedical Imaging* 2011 (2011), pp. 3–3.

[28] F. Bosi et al. "An elastica arm scale". In: *Proceedings of the Royal Society A: Mathematical, Physical and Engineering Sciences* 470.2169 (2014), p. 20140232.

[29] P. Koutsogiannakis et al. "Stabilization against gravity and self-tuning of an elastic variable-length rod through an oscillating sliding sleeve". In: *Journal of the Mechanics and Physics of Solids* 181 (2023), p. 105452.

[30] D. Bigoni et al. "Torsional locomotion". In: *Proceedings of the Royal Society A: Mathematical, Physical and Engineering Sciences* 470.2171 (2014), p. 20140599.

[31] F. Dal Corso et al. "Serpentine locomotion through elastic energy release". In: *Journal of the Royal Society Interface* 14.130 (2017), p. 20170055.

[32] A. Liakou and E. Detournay. "Constrained buckling of variable length elastica: Solution by geometrical segmentation". In: *International Journal of Non-Linear Mechanics* 99 (2018), pp. 204–217.

[33] R. Ballarini and G. Royer-Carfagni. "A Newtonian interpretation of configurational forces on dislocations and cracks". In: *Journal of the Mechanics and Physics of Solids* 95 (2016), pp. 602–620.

[34] N.N. Goldberg and O.M. O'Reilly. "A material momentum balance law for shells and plates with application to phase transformations and adhesion". In: *Acta Mechanica* 233.9 (2022), pp. 3535–3555.

[35] Z.-Q. Wang and E. Detournay. "Eshelbian force on a steadily moving liquid blister". In: *International Journal of Engineering Science* 170 (2022), p. 103591.

[36] T.K. Venkatadri, T. Henzel, and T. Cohen. "Torsion-induced stick-slip phenomena in the delamination of soft adhesives". In: *Soft Matter* 19.13 (2023), pp. 2319–2329.

[37] R. Wen et al. "Bending-activated biotensegrity structure enables female Megarhyssa to cross the barrier of Euler's critical force". In: *Science Advances* 9.42 (2023), eadi8284.

[38] F. Dal Corso, M. Amato, and D. Bigoni. "Elastic solids under frictionless rigid contact and configurational force". In: *Journal of the Mechanics and Physics of Solids* in press (2024).

[39] J. Donea et al. "Arbitrary Lagrangian–Eulerian Methods". In: *Encyclopedia of computational mechanics* (2004).

[40] R.A.K. Sanches and H.B. Coda. "On fluid–shell coupling using an arbitrary Lagrangian–Eulerian fluid solver coupled to a positional Lagrangian shell solver". In: *Applied Mathematical Modelling* 38.14 (2014), pp. 3401–3418.

[41] Y. Wang et al. "Arbitrary Lagrangian-Eulerian-type conserved discrete unified gas kinetic scheme for the simulations of transonic continuum and rarefied gas flows with moving boundaries". In: *Applied Mathematical Modelling* 113 (2023), pp. 545–572.

[42] Y. Zhang et al. "An efficient partitioned framework to couple Arbitrary Lagrangian-Eulerian and meshless vector form intrinsic finite element methods for fluid-structure interaction problems with deformable structures". In: *Applied Mathematical Modelling* 130 (2024), pp. 536–560.

[43] Y. Vetyukov. "Non-material finite element modelling of large vibrations of axially moving strings and beams". In: *Journal of Sound and Vibration* 414 (2018), pp. 299–317.

[44] J. Scheidl et al. "Mixed Eulerian–Lagrangian description in the statics of a flexible belt with tension and bending hanging on two pulleys". In: *PAMM* 18.1 (2018), e201800060.

[45] J. Scheidl et al. "Mixed Eulerian–Lagrangian shell model for lateral run-off in a steel belt drive and its experimental validation". In: *International Journal of Mechanical Sciences* 204 (2021), p. 106572.

[46] Ch. Schmidrathner, Y. Vetyukov, and J. Scheidl. "Non-material finite element rod model for the lateral run-off in a two-pulley belt drive". In: *ZAMM-Journal of Applied Mathematics and Mechanics/Zeitschrift für Angewandte Mathematik und Mechanik* 102.1 (2022), e202100135.

[47] E. Kocbay et al. "An enhanced stress resultant plasticity model for shell structures with application in sheet metal roll forming". In: *The International Journal of Advanced Manufacturing Technology* 130.1 (2024), pp. 781–798.

[48] L. Vu-Quoc and S. Li. "Dynamics of sliding geometrically-exact beams: large angle maneuver and parametric resonance". In: *Computer methods in applied mechanics and engineering* 120.1-2 (1995), pp. 65–118.

[49] A. Humer. "Dynamic modeling of beams with non-material, deformation-dependent boundary conditions". In: *Journal of sound and vibration* 332.3 (2013), pp. 622–641.

[50] J. Scheidl and Y. Vetyukov. "Review and perspectives in applied mechanics of axially moving flexible structures". In: *Acta Mechanica* 234.4 (2023), pp. 1331–1364.

[51] F. Boyer et al. "Extended Hamilton's principle applied to geometrically exact Kirchhoff sliding rods". In: *Journal of Sound and Vibration* 516 (2022), p. 116511.

[52] K. Behdinan, M.C. Stylianou, and B. Tabarrok. "Dynamics of flexible sliding beams—non-linear analysis part I: formulation". In: *Journal of Sound and Vibration* 208.4 (1997), pp. 517–539.

[53] D.B. McIver. "Hamilton's principle for systems of changing mass". In: *Journal of Engineering Mathematics* 7.3 (1973), pp. 249–261.

[54] N.A. Lemos. "Incompleteness of the Hamilton-Jacobi theory". In: *American Journal of Physics* 82.9 (2014), pp. 848–852.

[55] Y. Vetyukov and A. Humer. "Dancing rod problem in the context of Lagrangian mechanics". In: *EURODYN 2023: XXII International Conference on Structural Dynamics, July 2-5, 2023* (Delft, Netherlands). 2023.

[56] C. Armanini et al. "Configurational forces and nonlinear structural dynamics". In: *Journal of the Mechanics and Physics of Solids* 130 (2019), pp. 82–100. ISSN: 0022-5096.

[57] Sh. Han. "Configurational forces and geometrically exact formulation of sliding beams in non-material domains". In: *Computer Methods in Applied Mechanics and Engineering* 395 (2022), p. 115063.

[58] Sh. Han and O.A. Bauchau. "Configurational forces in variable-length beams for flexible multibody dynamics". In: *Multibody System Dynamics* 58.3-4 (2023), pp. 275–298.

[59] S. Bartels. "A simple scheme for the approximation of elastic vibrations of inextensible curves". In: *IMA Journal of Numerical Analysis* 36.3 (2016), pp. 1051–1071.

[60] S. Bartels and P. Reiter. "Numerical solution of a bending-torsion model for elastic rods". In: *Numerische Mathematik* 146 (2020), pp. 661–697.

[61] T.K. Papathanasiou. "A Linearised θ Numerical Scheme for the Vibrations of Inextensible Beams". In: *European Journal of Computational Mechanics* 30.1 (2021), pp. 121–144.

[62] P. Koutsogiannakis, T.K. Papathanasiou, and F. Dal Corso. *A simple ALE-FEM code in Matlab for structures with moving boundaries.* May 2024. URL: `https://github.com/pkouts/ale-fem-rod`.

[63] T.J.R. Hughes. *The Finite Element Method: Linear Static and Dynamic Finite Element Analysis.* Dover Civil and Mechanical Engineering. Dover Publications, 2012. ISBN: 9780486135021.

[64] A. Cazzolli and F. Dal Corso. "The elastica sling". In: *European Journal of Mechanics/A Solids* 105 (2024), p. 105273.

[65] A. Cazzolli and F. Dal Corso. "Snapping of elastic strips with controlled ends". In: *International Journal of Solids and Structures* 162 (2019), pp. 285–303.

[66] J. Liu, D. Yan, and Y. Zhang. "Mechanics of unusual soft network materials with rotatable structural nodes". In: *Journal of the Mechanics and Physics of Solids* 146 (2021), p. 104210.

[67] X. Huang et al. "The dominating dimensionless numbers of an elastic-plastic thin plate under dynamic loading". In: *Journal of the Mechanics and Physics of Solids* 186 (2024), p. 105593.